

國立交通大學

機械工程研究所

碩士論文

壓電致動器

在平面三自由度上精密定位

The Precise Positioning of 2-D and 3-DOF by

Piezoelectric actuator



研究生：許洋豪

指導教授：成維華 教授

中華民國九十七年七月

壓電致動器在平面三自由度上精密定位

The Precise Positioning of 2-D and 3-DOF

by Piezoelectric actuator

研究生：許洋豪

Student：Yang-Hao Hsu

指導教授：成維華

Advisor：Wei-Hua Chieng

國立交通大學

機械工程學系

碩士論文



Submitted to Institute of Mechanical Engineering
College of Engineering

National Chiao Tung University

in partial Fulfillment of the Requirements

for the Degree of

Master

in

Mechanical Engineering

July 2008

Hsinchu, Taiwan, Republic of China

中華民國九十七年七月

以壓電致動器進行平面三自由度之精密定位

研究生：許洋豪

指導教授：成維華 教授

國立交通大學機械工程學系

摘要

壓電致動器對於微步進機構是一種相當好的驅動器，有電量少、雜訊少、體積小、反應快、發熱少、精密度佳、轉換效率高和控制容易...等優點，本篇論文之微步進機構是利用壓電致動器對應驅動電壓反應快速的特性，並使用黏滯—滑動的摩擦機制，建構出可以用於精密定位的衝量驅動機構。我們首先以質量—阻尼—彈簧之衝量驅動機構做為分析此機構的動力學模型，並進行模擬。實驗則分為兩部分，首先探討不同驅動波形對同一機構所產生的步進現象有何差異，並對整個微步進機構進行系統鑑別。接著進行二維微步進機構之平移與旋轉實驗，來探討不同的驅動波型與機構移動的方式之間的關係，進一步使二維微步進機構的移動與期望的結果相符，並以人機介面提供使用者自由操作機構移動，以達到精密定位的目的。

The Precise Positioning of 2-D and 3-DOF by Piezoelectric Actuator

Student : Yang-Hao Hsu

Advisor : Dr. Wei-Hua Chieng

Institute of Mechanical Engineering
National Chiao Tung University

Abstract

Piezoelectric actuator is one better choice of actuator for micro-stepping mechanism because of low power consumption, low tolerance, less volume, rapid response, ultra-high resolution, high efficiency, low extra heat and easy control. This research use an impact drive mechanism (IDM) constructed by using the rapid displacement response of piezoelectric actuator and stick-slip motion of friction mechanism. We use a mass-damper-spring (MCK) model which is constructed to investigate the dynamics model of the mechanism and simulate this IDM system. The experiments are divided into two sections. We discuss the different between the same piezoelectric actuators but different driving waveforms first. And identify the whole micro-stepping mechanism system. It will help us to begin the next experiment. Next step is the experiment about translation and rotation of planar micro-steeping. We will find out the relations between the different waveforms and the displacement of the mechanism. Then we can control the micro-stepping motion satisfying our expectation. The human-computer interface will be constructed for user to bestride the mechanism stepping arbitrary and we achieve the purpose of precise positioning.

誌謝

首先,我要感謝我的指導老師，成維華教授。在我唸研究所的期間，老師在課業跟生活等方面，都給我許多很寶貴的意見，讓我獲益良多。也感謝前輩明欣學長對我在實驗材器的解說與實作。更感嘉豐學長，我對 IDM 的動力學理論完全陌生，就一直給予指導，一直到可以看懂方程式，或在實驗上有任何問題時兩肋插刀，鼎力相助。也感謝秉霖學長指導關於計畫書的撰寫，與做計畫流程的了解。實驗室的同學們，文彬，舶強，奕旻也在遇到困難時給予溫暖，實在非常感謝。感非常感謝學弟安鎮幫忙整理數據，節省了非常多的時間，也感謝學弟文祥、志隆、之浩、冠今更不時提供笑果，讓苦悶的研究生涯中，多了一點歡笑。最後感謝父母扶養，今天的任何成就，都要歸功於父母。

Contents

摘要	iii
Abstract	iv
誌謝	v
Contents	vi
Chapter 1	Introduction.....	1
1.1	Motive	1
1.2	History	1
1.3	Research orientation and objective	4
Chapter2	The dynamic model and simulation.....	6
2.1	Operating Principle of Impact Drive Mechanism	6
2.2	The Model of 1-D system	8
2.3	The Model of 2-D and 3-DOF system	18
Chapter 3	The experiment and data acquisition of 2-D IDM.....	26
3.1	Experimental Equipment	26
3.2	Experimental Results	30
Chapter 4	Conclusion.....	33
Reference	35
List of Figures	38
List of Tables	62

Chapter 1 Introduction

1.1 Motive

Piezoelectric material is a special substance which is one better choice of actuator for micro-stepping mechanism because of low power consumption, low tolerance, less volume, rapid response, ultra-high resolution, high efficiency, low extra heat and easy control. Nevertheless, they are not diffusive and popular in commercial because of the expensive cost and the limited stroke. Otherwise, the common precise positioning technique requires two-stage to move to the position we desired. But the piezoelectric IDM actuator has just one stage to position. Due to the reason above, there is illimitable perspective to research and develop.



1.2 History

In 1880, brothers; Pierre and Jacques Curie, predicted and demonstrated a related phenomenon using tinfoil, glue, wire, magnets, and a jeweler's saw. They showed that crystals of tourmaline, quartz, topaz, cane sugar, and Rochelle salt generate electrical polarization from mechanical stress. There are many applications via this.

Many types of piezoelectric precision positioning systems have been proposed for industrial and scientific applications. Figure 1.1 lists the typical classifications of these systems. Scanning devices produce motion by direct driven or mechanical amplified. Pulse devices include stick-slip and other types of clamping mechanism. The stick-slip device which is

based on the rapid response of continuous driving voltage can generate stable stepping motion from mechanical excitation of the piezoelectric device. The stick-slip behavior results from the contact friction between the movable part and the guide surface. The third type of piezoelectric positioning system is the ultrasonic motor. The acoustic wave produced by resonantly excite piezoelectric materials induces the mechanical movement.

There are many related paper discussing the IDM. S. Ling et al [1] developed a piezoelectric linear motor. They presented a push-pull type of 1-D linear motor. An analytical model for such a linear motor system was developed. Higuchi et al [2] proposed a prototype IDM and applied it in the design of a micro robot that serves as an inserted capillary in a cell-operation. J.MEDES et al [3] use IDM to position a printed board. A device for three degree of freedom precision positioning using IDM and a closed-loop feedback system has been presented. The stick-slip operation of IDM is dominated by the energy dissipation of the system, some of which results from the contact friction between the slider and the guide surface. K. Furutani et al. studied the effect of lubrication on IDM [4]. They discussed the motion of IDM based on Newton mechanics. An approximate estimate of the motion of IDM under a specific exciting waveform pattern was provided. Four guide-surface conditions – dry, lubricated by EDF-K, Oil 32 and Oil 68 – were experimentally studied. Surface condition did not apparently affect the behavior of IDM. The critical effect of the dissipation of energy in the system is not discussed. The application of IDM to multi D.O.F. positioning has also been extensively discussed. J. Mendes et al. constructed a planar positioning

machine to finely position a print board on a work plane [3]. They used a group of six IDMs in a plane to push a work piece in the X and Y directions. The path planning of the work piece which uses six actuators was performed. Image feedback was used to achieve closed-loop position control. The mechanism was based on the robotic “Pushing Operation” of M. Mason et al. [5][6][8]. Y. Yamagata et al. proposed a similar approach [7]. They used a multi D.O.F. IDM on the end effector of a robot arm to perform automatic, precise assembly. K. Furutani et al. used IDM to develop a precision electrical discharge machine (EDM) [9][10]. They constructed an X-Y-Z- θ movable electrode-feeding device. The electrode was carried with the planar IDM. The path planning of the planer IDM-driven electrode was also accomplished.

Many clamping mechanisms were introduced to “increase” the friction force between the slider and the guide surface during the “sticking phase” of the operation of IDM to improve the poor controllability and repeatability of the stick-slip motion. K. Ikuta et al. proposed a kind of IDM using electromagnetic clamping [11]. The slider is electromagnetically clamped during the sticking phase and released during the slip phase. An extra D.O.F. of control of the electromagnetic coil was introduced. T. Idogaki et al. used a preload spring to clamp the slider to the guide surface of IDM [12]. The passive preload exerts a larger normal force between the contact surface of the slider and the guide of IDM.

The piezoelectric material-based IDM was selected as the precise positioning in this research. The following sections emphasize on the operation and stepping behavior of IDM.

1.3 Research orientation and objective

The mechanism is a modified impact drive mechanism (IDM) which belongs to the stick slip device of pulse type. The general operating principle of IDM is to apply asymmetric voltage waveform to PZT. The sketch of Figure 1.2 demonstrates the mechanism. The PZT actuator is connected between slider and counter-mass of IDM and then the IDM causes a series of stick-slip motion powered by PZT actuator on the guide way. Three PZT actuators on a circular plate will compose a planar, 3-DOF IDM mechanism see Figure 1.3. The detail motion principle of IDM will be mentioned in CH2-1. CH2-2 and CH2-3 described the 1D-1DOF and 2D-3DOF mass-damper-spring model combined with friction model is adopted to investigate the dynamics of the mechanism. The simulations by Matlab Simulink are also presented.

In CH3, we will introduce the positioning experiment. We input the waveform derived and simulated by CH2 which include the following constrains:

1. Forward or backward waveform.
2. Frequency.
3. Amplitude. (The stroke of PZT actuators)

The goal for we to achieve is establishing human-computer interface. Users can see the actuator's position by a monitor. They can bestride the whole mechanism by joystick or keyboard. We have to establish six control units as following:

1. Unit positive X-directional stepping.
2. Unit negative X-directional stepping.

3. Unit positive Y-directional stepping.
4. Unit negative Y-directional stepping.
5. Unit positive θ -directional stepping.
6. Unit negative θ -directional stepping.

The goal stepping size above is $0.2\mu\text{m}$. This order of precision can satisfy our applications. Users can compose the above units moving to arbitrary position. The processing will present in CH3. CH4 denotes the conclusion of this dissert.



Chapter 2 System Dynamic Model and Simulation

2.1 Operating Principle of Impact Drive Mechanism

Impact drive mechanism (IDM) means the motion of the actuators driving by inertia force. The mechanism consists of three elements: the main mass, a piezoelectric element and a counter-mass. Figure 2.1 describes the input waveform pattern corresponding to the movement of one dimensional linear positioning device. The slider is put on a surface and held by the friction force. A counter-mass is connected to the main object via one piezoelectric element. Controlling extension or contraction of the piezoelectric actuator by applying voltage waveforms to the piezoelectric actuator, the mechanism will move step by step. Figure 2.1 (a) represents a control method of deformations of the piezoelectric actuator for backward movement.

(1) A movement cycle begins with the original length of the piezoelectric actuator and the mechanism is stationary at start.

(2) A steep rising voltage is applied. The piezoelectric actuator makes a rapid extension and the slider moves backward and the counter-mass forward.

(3) While returning, the counter-mass should be accelerated by a constant acceleration which causes inertial force less than the static friction force. Otherwise, the slider makes reverse movement.

(4) By the time the piezoelectric actuator is contracted to the length of the beginning, a sudden stop is happened. This action is just like a collision of the counter-mass and the slider. So the whole system starts moving backward against friction force until it loses its kinetic energy.

(5) IDM stops and the piezoelectric actuator recovers itself.

The cycle is completed through (1) to (5). Therefore, IDM can move a long distance by repeating this cycle. The same may be said, no doubt, of forward movement as shown in Figure 2.1 (b).

(1) A movement cycle begins with the original length of the piezoelectric actuator and the mechanism is stationary at start.

(2) A gentle rising voltage is applied. The piezoelectric actuator extends and the slider keeps stationary because counter-mass should be accelerated by a constant acceleration which causes inertial force less than the static friction force.

(3) While returning, a steep rising voltage is applied. The piezoelectric actuator makes a rapid contraction and the slider moves forward and the counter-mass backward.

(4) By the time the piezoelectric actuator is original length, a sudden stop is happened. Then a steep decreasing voltage is applied. This action which happened in the moment of change of applied voltage is just like a hammer to hit the slider.

(5) IDM stops and the piezoelectric actuator recovers itself.

These all above are the operation of one-dimensional impact drive mechanism about how to move forward and backward. It is similar to the two-dimensional impact drive mechanism. The difference between one-dimension IDM and two-dimension is that the same asymmetrical triangle voltage waveform applied to one-dimension can produce linear movement only, but it applied to two-dimension IDM can produce translation and rotational movement. So we want to control the movement of the two-dimension IDM, we need to know the difference

between three actuators about the same and different input waveform.

2.2 The Model of 1-D system

2.2.1 The rigid-body Model of 1-D IDM

In usual case, F_1 is frictional force F_μ and F_2 is equal to zero. The rigid-body model is shown in Figure 2.2. The motion equation by free body diagrams are expressed as follows:

$$\begin{cases} M\ddot{x}_1 = F_p + f \\ m\ddot{x}_2 = -F_p \end{cases} \quad (2.1)$$

M and m denote the mass of slider and counter-mass separately. F_p denotes the force between counter-mass and slider. f denotes the friction force between slider and guide plane. x_1 and x_2 denote the positions of slider and counter-mass separately. Because of the rigid body assumption, we can denote that:

$$x_2 = x_1 + l \quad (2.2)$$

We can solve \ddot{x}_1 by taking the second derivatives of equation (2.2), and substitute into equation (2.1).

$$\ddot{x}_1 = \frac{f - m\ddot{l}}{m + M} = \frac{f}{m + M} - \frac{m\ddot{l}}{m + M} \quad (2.3)$$

Equation (2.3) will separate into 2 cases.

Case 1: If the velocity of slider is not zero, friction force f equals the

product of normal force and kinetic friction coefficient. We can write that:

$$\dot{x}_1 = \int \frac{f dt}{m+M} - \frac{ml}{m+M} = \mu g t - \frac{ml}{m+M} \quad (2.4)$$

Case 2: If the velocity of slider is zero, friction force depends on the result of comparison. If force $m\ddot{u}$ is larger than the maximum static force, friction force equals kinetic friction force. If force $m\ddot{u}$ is smaller than the maximum static force, friction force equals $m\ddot{u}$. So that total force is zero. Slider remains at rest. The friction force always affects the slider velocity tending to zero.

Input waveform u is asymmetric wave shown in Figure 2.3(a). Figure 2.3(b) shows the first derivative of input waveform. The velocity function is always horizontal. That is, the velocity change is very fast. Figure 2.3(c) shows the second term of equation (2.4). We can see the velocity change as impulse action which is shown in Figure 2.3(c). The impulse force is larger than maximum static friction force absolutely that case 2 is invalid. Since all parameter are known, equation 2.4 can be solved and drawn as figure 2.4(a). Figure 2.4(b) shows the position of slider be solved by integrating equation 2.4. The displacement from second step is result of lower trapezoid area ABCD subtracting upper triangle area DEF in Figure 2.5. Triangle DEF and triangle GBC is congruent because:

$$\begin{aligned} \angle CGB &= \angle FDE = 90^\circ \\ \angle GCB &= \angle DFE = \tan^{-1}(\mu g) \\ \overline{GB} &= \overline{DE} = \mu g T \gamma \end{aligned}$$

Step size is area of ADCG in Figure 2.5. That is:

$$\begin{aligned}
&= \left(\frac{rS}{T(1-\gamma)} + \frac{rS}{T\gamma} - \mu g T \gamma \right) T \gamma \\
&= rS \left(\frac{1}{1-\gamma} \right) - \mu g T^2 \gamma^2
\end{aligned} \tag{2.5}$$

The step size is derived above. However this is rigid body case. There are many factors of Piezo-actuators that we can't neglect. Following is discussing of mass-damper-spring model instead of the rigid body mode.

2.2.2 The mass-damper-spring Model of 1-D IDM

In usual case, F_1 is frictional force F_μ and F_2 is equal to zero. The mass-damper-spring model of IDM shown in Figure 2.6 is expressed as follows:

$$\begin{cases} M\ddot{x}_1 + c(\dot{x}_1 + \dot{l} - \dot{x}_2) + k(x_1 + l - x_2) = F_\mu \\ m\ddot{x}_2 + c(\dot{x}_2 - \dot{l} - \dot{x}_1) + k(x_2 - l - x_1) = 0 \end{cases} \tag{2.6}$$

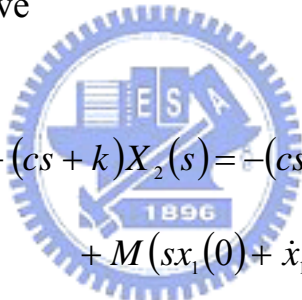
The piezoelectric actuator is considered to be linear and rigid. According to the design of the piezoelectric actuator, the mechanical interface between the slider and the counter-mass is specified as a linear spring constant k and a linear damping coefficient c . Assuming no contact friction between the counter-mass and the guide way, there is only one friction between the slider and the guide way. The variables x_1 , x_2 represent the displacement of the slider, the counter-mass and the piezoelectric actuator respectively. In rigid body case, $x_2 = x_1 + l$. But now, the input l is connecting with damper and spring. M and m

are the mass of the slider and the counter-mass.

In a more general case shown in figure 2.7 , external forces act on the slider and the counter-mass (frictional force, magnetic clamping force, etc.), the mass-damper-spring model for the system turns into

$$\begin{cases} M\ddot{x}_1 + c(\dot{x}_1 + \dot{l} - \dot{x}_2) + k(x_1 + l - x_2) = F_1 \\ m\ddot{x}_2 + c(\dot{x}_2 - \dot{l} - \dot{x}_1) + k(x_2 - l - x_1) = F_2 \end{cases} \quad (2.7)$$

where F_1 and F_2 represent the external force on the slider and the counter-mass respectively. By taking the Laplace transform for both sides of above equations, we have



$$\begin{aligned} (Ms^2 + cs + k)X_1(s) - (cs + k)X_2(s) &= -(cs + k)L(s) + F_1(s) \\ &\quad + M(sx_1(0) + \dot{x}_1(0)) + c(x_1(0) - x_2(0) + l(0)) \\ -(cs + k)X_1(s) + (ms^2 + cs + k)X_2(s) &= (cs + k)L(s) + F_2(s) \\ &\quad + m(sx_2(0) + \dot{x}_2(0)) + c(x_2(0) - x_1(0) - l(0)) \end{aligned} \quad (2.8)$$

The above algebraic equations can be solved as

$$\begin{bmatrix} X_1 \\ X_2 \end{bmatrix} = \frac{1}{s^2(Mms^2 + c(M + m)s + k(M + m))} \cdot \begin{bmatrix} ms^2 + cs + k & cs + k \\ cs + k & Ms^2 + cs + k \end{bmatrix} \begin{bmatrix} -(cs + k)L + F_1 + I_1 \\ (cs + k)L + F_2 + I_2 \end{bmatrix} \quad (2.9)$$

Where $I_1 = Mx_1(0)s + I_{10}$ and $I_2 = mx_2(0)s + I_{20}$ represents the terms which contain the initial conditions of the system. We can rewrite the vector $[X_1 \ X_2]^T$ composed of 5 separated vectors.

$$\begin{bmatrix} X_1 \\ X_2 \end{bmatrix} = \begin{bmatrix} X_{1,L} \\ X_{2,L} \end{bmatrix} + \begin{bmatrix} X_{1,F1} \\ X_{2,F1} \end{bmatrix} + \begin{bmatrix} X_{1,F2} \\ X_{2,F2} \end{bmatrix} + \begin{bmatrix} X_{1,I1} \\ X_{2,I1} \end{bmatrix} + \begin{bmatrix} X_{1,I2} \\ X_{2,I2} \end{bmatrix} \quad (2.10)$$

Where subscript L , $F1$ and $F2$ represent the effect of piezoelectric element, external forces act on the slider and the counter-mass. $I1$ and $I2$ represent the effect of the initial conditions of the system. The individual quantity can be obtained as follows.

$$\begin{cases} X_{1,L} = \frac{-m(cs+k) \cdot L(s)}{Mms^2 + c(M+m)s + k(M+m)} = G_{L1}(s)L(s) \\ X_{2,L} = \frac{M(cs+k) \cdot L(s)}{Mms^2 + c(M+m)s + k(M+m)} = G_{L2}(s)L(s) \end{cases} \quad (2.11)$$

$$\begin{cases} X_{1,F1} = \frac{(ms^2 + cs + k) \cdot F_1(s)}{s^2(Mms^2 + c(M+m)s + k(M+m))} = G_{F11}(s)F_1(s) \\ X_{2,F1} = \frac{(cs + k) \cdot F_1(s)}{s^2(Mms^2 + c(M+m)s + k(M+m))} = G_{F12}(s)F_1(s) \end{cases} \quad (2.12)$$

$$\begin{cases} X_{1,F2} = \frac{(cs + k) \cdot F_2(s)}{s^2(Mms^2 + c(M+m)s + k(M+m))} = G_{F21}(s)F_2(s) \\ X_{2,F2} = \frac{(Ms^2 + cs + k) \cdot F_2(s)}{s^2(Mms^2 + c(M+m)s + k(M+m))} = G_{F22}(s)F_2(s) \end{cases} \quad (2.13)$$

$$\begin{cases} X_{1,I1} = \frac{(ms^2 + cs + k) \cdot (Mx_1(0)s + I_{10})}{s^2(Mms^2 + c(M+m)s + k(M+m))} \\ X_{2,I1} = \frac{(cs + k) \cdot (Mx_1(0)s + I_{10})}{s^2(Mms^2 + c(M+m)s + k(M+m))} \end{cases} \quad (2.14)$$

$$\begin{cases} X_{1,I2} = \frac{(cs + k) \cdot (mx_2(0)s + I_{20})}{s^2(Mms^2 + c(M+m)s + k(M+m))} \\ X_{2,I2} = \frac{(Ms^2 + cs + k) \cdot (mx_2(0)s + I_{20})}{s^2(Mms^2 + c(M+m)s + k(M+m))} \end{cases} \quad (2.15)$$

By the inverse Laplace transform $L^{-1}\{\cdot\}$ the displacement of the slider under actuation of IDM can be obtained as

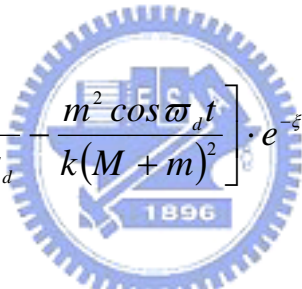
$$\begin{aligned} x_1(t) = & L^{-1}\{G_{L1}(s)L(s)\} + L^{-1}\{G_{F11}(s)F_1(s)\} + L^{-1}\{G_{F21}(s)F_2(s)\} \\ & + L^{-1}\{X_{1,I1}(s)\} + L^{-1}\{X_{2,I2}(s)\} \end{aligned} \quad (2.16)$$

In the following formulations, we assume the load capacity of piezoelectric element is large enough and the output is corresponding to the rapid deflection stage or the slow deflection stage of the piezoelectric element only. The displacement of slider drive previously can be rewritten as

$$x_{1,L} = \frac{mL_{max} \sin \varpi_d t \cdot e^{-\xi \varpi_n t}}{\beta T (M+m) \varpi_d} - \frac{mL_{max}}{M+m} \frac{t}{\beta T} \quad (2.17)$$

$$x_{2,L} = \frac{-ML_{max} \sin \varpi_d t \cdot e^{-\xi \varpi_n t}}{\beta T (M+m) \varpi_d} + \frac{ML_{max}}{M+m} \frac{t}{\beta T} \quad (2.18)$$

where β represents the percentage of the slanting stage in a cycle (γ or $1-\gamma$); L_{max} represents the maximum deflection of the piezoelectric element; γ and T are the complement duty cycle and the period of triangular waveform respectively. Similarly, we can obtain the relation between the displacement of the slider and external constant forces F_1 and F_2 as follows.



$$x_{1,F1}(t) = \left\{ \left[\frac{-cm \sin \varpi_d t}{2kM(M+m)\varpi_d} - \frac{m^2 \cos \varpi_d t}{k(M+m)^2} \right] \cdot e^{-\xi \varpi_n t} + \frac{m^2}{k(M+m)^2} + \frac{t^2}{2(M+m)} \right\} F_1$$

$$x_{2,F1}(t) = \left\{ \left[\frac{c \sin \varpi_d t}{2k(M+m)\varpi_d} + \frac{Mm \cos \varpi_d t}{k(M+m)^2} \right] \cdot e^{-\xi \varpi_n t} - \frac{Mm}{k(M+m)^2} + \frac{t^2}{2(M+m)} \right\} F_1$$

$$x_{1,F2}(t) = \left\{ \left[\frac{c \sin \varpi_d t}{2k(M+m)\varpi_d} + \frac{Mm \cos \varpi_d t}{k(M+m)^2} \right] \cdot e^{-\xi \varpi_n t} - \frac{Mm}{k(M+m)^2} + \frac{t^2}{2(M+m)} \right\} F_2$$

$$x_{2,F2}(t) = \left\{ \left[\frac{-Mc \sin \varpi_d t}{2km(M+m)\varpi_d} - \frac{M^2 \cos \varpi_d t}{k(M+m)^2} \right] \cdot e^{-\xi \varpi_n t} + \frac{M^2}{k(M+m)^2} + \frac{t^2}{2(M+m)} \right\} F_2$$

Finally, the initial condition of slider displacement and counter-mass displacement for each stage are

$$x_{1,i1}(t) = \left[\frac{2mI_{10} - c(M+m)x_1(0)}{2M(M+m)\varpi_d} \sin \varpi_d t + \frac{mx_1(0)}{M+m} \cos \varpi_d t \right] e^{-\xi\varpi_n t} + \frac{Mx_1(0) + I_{10}t}{M+m}$$

$$x_{2,i1}(t) = \left[\frac{c(M+m)x_1(0) - 2mI_{10}}{2m(M+m)\varpi_d} \sin \varpi_d t - \frac{Mx_1(0)}{M+m} \cos \varpi_d t \right] e^{-\xi\varpi_n t} + \frac{Mx_1(0) + I_{10}t}{M+m}$$

$$x_{1,i2}(t) = \left[\frac{c(M+m)x_2(0) - 2MI_{20}}{2M(M+m)\varpi_d} \sin \varpi_d t - \frac{mx_2(0)}{M+m} \cos \varpi_d t \right] e^{-\xi\varpi_n t} + \frac{mx_2(0) + I_{20}t}{M+m}$$

$$x_{2,i2}(t) = \left[\frac{2MI_{20} - c(M+m)x_2(0)}{2m(M+m)\varpi_d} \sin \varpi_d t + \frac{Mx_2(0)}{M+m} \cos \varpi_d t \right] e^{-\xi\varpi_n t} + \frac{mx_2(0) + I_{20}t}{M+m}$$

From above formulation, we can conclude the characteristic of IDM as a second order dynamic system with damped natural frequency and damping ratio as follows.

$$\varpi_d = \varpi_n \sqrt{1 - \xi^2} = \frac{1}{2Mm} \sqrt{(M+m)[4kMm - c^2(M+m)]} \quad (2.19)$$

$$\xi\varpi_n = \frac{c(M+m)}{2Mm} \quad (2.20)$$

$$\xi = \frac{c(M+m)}{\sqrt{4kMm(M+m)}} = \frac{c}{2} \sqrt{\frac{M+m}{kMm}} \quad (2.21)$$

2.2.2 System identification of 1-D IDM Model

The parameters of the proposed model must be estimated from the experimentally measured data to predict the behavior of the mechanism precisely enough. As described in the preceding sections, a model of IDM with a linearization MCK system consists of a Coulomb friction model and a linear actuator; three parameters are required. The estimated parameters include the stiffness k , the damping coefficient c of the piezoelectric actuator and the frictional coefficient μ . First we use the model like Figure 2.8 to estimate the stiffness and the damping coefficient. A finite difference approximation to the MCK system is used to discretize the dynamics of the slider and the count-mass of the mechanism. The discretized system is specified as follows.

$$(x_i - 2x_{i-1} + x_{i-2}) + \frac{c}{m} \Delta(x_i - x_{i-1} - u_i + u_{i-1}) + \frac{k}{m} \Delta^2(x_i - u_i) = 0 \quad (2.22)$$

Then the equation of the discretized system can be rearranged as follows.

$$Hw - y = 0$$

$$\text{where } \begin{cases} H = [x_i - x_{i-1} - u_i + u_{i-1} & x_i - u_i] \\ w = \begin{bmatrix} \frac{c}{m} \Delta & \frac{k}{m} \Delta^2 \end{bmatrix}^T \\ y = -(x_i - 2x_{i-1} + x_{i-2}) \end{cases} \quad (2.23)$$

A weighted least square algorithm is used to make sure that the identified parameters properly converge to a range. w is the a matrix that contain the parameters what we want to estimate. The final goal is to estimate the stiffness and the damping coefficient by iteration of w and then minimizing the value of $\|Hw - y\|$. The equations of WRLS are shown as follows:

$$\min_w \|Hw - y\| \quad (2.24)$$

$$P_i = \lambda_i \left[P_{i-1} - \frac{P_{i-1} h_i^* h_i P_{i-1}}{\lambda_i + h_i P_{i-1} h_i^*} \right], P_0 = I$$

$$w_i = w_{i-1} + \frac{P_{i-1} h_i^*}{\lambda_i + h_i P_{i-1} h_i^*} (y_i - h_i w_{i-1})$$

λ_i is equal to 0.999 to perform a forgetting factor for the system identification

The result of parameter estimation is shown as Figure 2.9. The upper diagram of Figure 2.10 is the input of actuator and the lower is the output. The stiffness is about 10^7 and the damping coefficient is 180.

2.2.3 The Simulation of 1-D Model

Simulink is a platform for multi-domain simulation and Model-Based Design for dynamic systems. It provides an interactive graphical environment and a customizable set of block libraries, and can be extended for specialized applications. We simulate the rigid body model and mass-damper-spring model by the Simulink separately. The rules of connection follow the equations of the mass-damper-spring model. The results of simulation are shown as Figure 2.11.

2.3 The Model of 2-D and 3-DOF system

This model is derived by Lagrange method. The method derives the system equations by energy conception.

2.3.1 The mass-damper-spring model of 2-D IDM

Lagrange's equation is fundamental relation in Lagrange's mechanics given by

$$\frac{d}{dt} \left(\frac{\partial L}{\partial \dot{q}_i} \right) - \frac{\partial L}{\partial q_i} + \frac{\partial D}{\partial \dot{q}_j} = Q_j \quad (2.25)$$

where q_j is a general coordinate, Q_j is the general work, D is the energy absorbed by damper and L is the Lagrangian.

$$L \equiv T - U \quad (2.26)$$

where T is the total kinetic energy and U is the total potential energy.

The kinetic energy include the energy resulted from the movement of the plate and the three count-mass. Based on our assumption the terms of energy are shown as follows behind calculation.

$$\begin{aligned} T &= \frac{1}{2} M \dot{x}^2 + \frac{1}{2} M \dot{y}^2 + \frac{1}{2} I \dot{\theta}^2 + \sum_i \frac{1}{2} m_i (\dot{x}^2 + \dot{y}^2) + \sum_j \frac{1}{2} m_j (\dot{d}_j - R_j \dot{\theta})^2 \\ &\quad + \sum_i m_i (\dot{d}_i - R_i \dot{\theta}) \left[\dot{x} \sin(\phi_i + \theta) - \dot{y} \cos(\phi_i + \theta) \right] \\ U &= \sum_i \frac{1}{2} k_i (d_i - u_i)^2 \\ &\quad + \sum_i \frac{1}{2} c_i (\dot{d}_i - \dot{u}_i)^2 \end{aligned} \quad (2.27)$$

To substitute the three terms into the equation 2.26 and to calculate the equations can make us to obtain the model of IDM. The mass-damper-spring model of IDM shown in Figure2.12 is expressed as

follows:

$$\left\{ \begin{array}{l} M\ddot{x} + \sum_i m_i \ddot{x} + \sum_i m_i (\ddot{d}_i - R_i \ddot{\theta}) \sin(\theta + \phi_i) + \sum_i m_i (\dot{d}_i \dot{\theta} - R_i \dot{\theta}^2) \cos(\theta + \phi_i) = F_{\mu x} \\ M\ddot{y} + \sum_i m_i \ddot{y} - \sum_i m_i (\ddot{d}_i - R_i \ddot{\theta}) \cos(\theta + \phi_i) + \sum_i m_i (\dot{d}_i \dot{\theta} - R_i \dot{\theta}^2) \sin(\theta + \phi_i) = F_{\mu y} \\ I\ddot{\theta} - \sum_i m_i R_i (\ddot{d}_i - R_i \ddot{\theta}) - \sum_i m_i \ddot{x} R_i \sin(\theta + \phi_i) + \sum_i m_i \ddot{y} R_i \cos(\theta + \phi_i) \\ \quad - \sum_i m_i \dot{x} \dot{d}_i \cos(\theta + \phi_i) - \sum_i m_i \dot{y} \dot{d}_i \sin(\theta + \phi_i) = M_{\mu} \\ m_i \ddot{x} \sin(\theta + \phi_i) - m_i \ddot{y} \cos(\theta + \phi_i) + m_i \dot{x} \dot{d}_i \cos(\theta + \phi_i) + m_i \dot{y} \dot{d}_i \sin(\theta + \phi_i) \\ \quad + m_i \ddot{d}_i - m_i R_i \ddot{\theta} + c_i (\dot{d}_i - \dot{u}_i) + k_i (d_i - u_i) = 0 \end{array} \right. \quad (2.28)$$

The Coulomb frictional force and moment between the slider and guide surface are composition of magnitude and direction. The magnitude of frictional force always equals the product of friction coefficient and normal force if velocity is non zero. The direction of frictional force equals opposite direction of motion direction. Frictional force and moment can estimate by multiplying magnitude and directions.

The contact between mechanics and surface are three screws shown as Figure 3.11. We see the contact between mechanics and surface are only three points. The coordinates of three points P_A, P_B, P_C are following:

$$\begin{aligned} P_A &= (x' - r \cdot \sin(\theta + 90^\circ))i + (y' + r \cdot \cos(\theta + 90^\circ))j \\ P_B &= (x' - r \cdot \sin(\theta + 210^\circ))i + (y' + r \cdot \cos(\theta + 210^\circ))j \\ P_C &= (x' - r \cdot \sin(\theta + 330^\circ))i + (y' + r \cdot \cos(\theta + 330^\circ))j \end{aligned} \quad (2.29a)$$

x' and y' represents the coordinates of center of total mass. Then we take the derivatives of equation 2.29a, we can write that:

$$\begin{aligned}
v_A &= (\dot{x}' - \omega \cdot r \cdot \sin(\theta + 90^\circ))i + (\dot{y}' + \omega \cdot r \cdot \cos(\theta + 90^\circ))j \\
v_B &= (\dot{x}' - \omega \cdot r \cdot \sin(\theta + 210^\circ))i + (\dot{y}' + \omega \cdot r \cdot \cos(\theta + 210^\circ))j \\
v_C &= (\dot{x}' - \omega \cdot r \cdot \sin(\theta + 330^\circ))i + (\dot{y}' + \omega \cdot r \cdot \cos(\theta + 330^\circ))j
\end{aligned}
\tag{2.29b}$$

\dot{x}' and \dot{y}' represents the first derivatives of velocity at mass center in x direction and y direction. ω represents the rotation velocity around mass center. r represent the distance of mass center and contact point. The magnitude of friction force at point A is:

$$\frac{1}{3} \cdot \mu_k \cdot (M + 3m) \cdot g
\tag{2.30}$$

The direction of friction force at point A is:

$$-\left(\frac{v_{Ax}i + v_{Ay}j}{\sqrt{v_{Ax}^2 + v_{Ay}^2}} \right)
\tag{2.31}$$



The negative sign represents frictional forces are opposite of motion direction. Similarity, the contact points B and C can be known. The total friction force about mass center is sum of three contact points. The moment about center mass is the cross product of r and frictional force about point A, that is $\overline{GA} \times f_A$ shown in figure 2.13. We can rearrange as following:

$$\begin{aligned}
F_{\mu x} &= -\frac{1}{3} \cdot \mu_k \cdot (M + 3m) \cdot g \cdot \left(\frac{v_{Ax}}{\sqrt{v_{Ax}^2 + v_{Ay}^2}} + \frac{v_{Bx}}{\sqrt{v_{Bx}^2 + v_{By}^2}} + \frac{v_{Cx}}{\sqrt{v_{Cx}^2 + v_{Cy}^2}} \right) \\
F_{\mu y} &= -\frac{1}{3} \cdot \mu_k \cdot (M + 3m) \cdot g \cdot \left(\frac{v_{Ay}}{\sqrt{v_{Ax}^2 + v_{Ay}^2}} + \frac{v_{By}}{\sqrt{v_{Bx}^2 + v_{By}^2}} + \frac{v_{Cy}}{\sqrt{v_{Cx}^2 + v_{Cy}^2}} \right) \\
M_{\mu} &= r \cdot \cos(\theta + 90^\circ) \cdot \frac{-v_{Ay}}{\sqrt{v_{Ax}^2 + v_{Ay}^2}} + r \cdot \sin(\theta + 90^\circ) \cdot \frac{v_{Ax}}{\sqrt{v_{Ax}^2 + v_{Ay}^2}} + \\
& r \cdot \cos(\theta + 210^\circ) \cdot \frac{-v_{By}}{\sqrt{v_{Bx}^2 + v_{By}^2}} + r \cdot \sin(\theta + 210^\circ) \cdot \frac{v_{Bx}}{\sqrt{v_{Bx}^2 + v_{By}^2}} + \\
& r \cdot \cos(\theta + 330^\circ) \cdot \frac{-v_{Cy}}{\sqrt{v_{Cx}^2 + v_{Cy}^2}} + r \cdot \sin(\theta + 330^\circ) \cdot \frac{v_{Cx}}{\sqrt{v_{Cx}^2 + v_{Cy}^2}}
\end{aligned} \tag{2.32}$$

Because the affect of the terms about Coriolis Force is not obvious, these equations can be rearranged as follows:

$$\left\{ \begin{aligned}
M\ddot{x} + \sum_i m_i \ddot{x} + \sum_i m_i (\ddot{d}_i - R_i \ddot{\theta}) \sin(\theta + \phi_i) &= F_{\mu x} \\
M\ddot{y} + \sum_i m_i \ddot{y} - \sum_i m_i (\ddot{d}_i - R_i \ddot{\theta}) \cos(\theta + \phi_i) &= F_{\mu y} \\
I\ddot{\theta} - \sum_i m_i R_i (\ddot{d}_i - R_i \ddot{\theta}) - \sum_i m_i \ddot{x} R_i \sin(\theta + \phi_i) + \sum_i m_i \ddot{y} R_i \cos(\theta + \phi_i) &= M_{\mu} \\
m_i \ddot{x} \sin(\theta + \phi_i) - m_i \ddot{y} \cos(\theta + \phi_i) + m_i \ddot{d}_i - m_i R_i \ddot{\theta} \\
+ c_i (\dot{d}_i - \dot{u}_i) + k_i (d_i - u_i) &= 0
\end{aligned} \right. \tag{2.33}$$

According to the assumption in section 2.2, the mechanical interface between the slider and the counter-mass is specified as a linear spring constant k_i and a linear damping coefficient c_i . There is no contact friction between the counter-mass and the guide surface but the slider and

guide surface. The variables x , y represent the displacements of the mechanism in X-axis and Y-axis. θ represents the rotation of the mechanism. ϕ_i represents the angle between the place where the actuator fastened on and the X'-axis. u_i and d_i are the inputs and the displacement of count-mass respect to the mechanism.

The first three equations are dynamic equations and the others are constraints. These equations are very complicated and nonlinear and cannot be decoupled. It is very difficult to solve these equations directly but numerical methods seem to be better way to solve these equations. To analyze the dynamics of the 2-D micro-stepping mechanism by numerical method need accurate data including the stiffness k_i , damping coefficient c_i of the actuators, the frictional coefficient μ between the mechanism and guide surface and so on. Those data need to be estimated by a series of experiments.

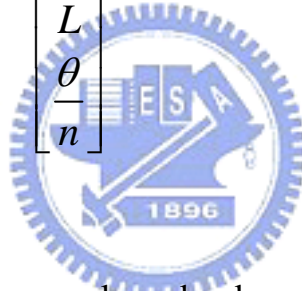
2.3.2 The control input

According to the results of 1-D IDM, we know that IDM motions step by step. We assume that each stepping motions are powered by a pretend force vector. The vector can be decomposed into x and y directions. If input unit pretend force, the IDM mass center will causing a distance L displacement and a angle θ rotation. Furthermore, we assume the linearity of pretend force. That is 2 times magnitude of pretend force will causing 2 times displacement and rotation. According above hypothesis, we can write that:

$$\begin{aligned}
a_1L + a_2L \cos(120^\circ) + a_3L \cos(240^\circ) &= x \\
a_2L \sin(120^\circ) + a_3L \sin(240^\circ) &= y \\
a_1n + a_2n + a_3n &= \theta
\end{aligned}
\tag{2.34}$$

a_1, a_2, a_3 represents the three coefficients of PZT. We just input some coefficients appropriate for the direction of movement we want. Above equation can be written as matrix form as following.

$$\begin{bmatrix} 1 & -0.5 & -0.5 \\ 0 & \frac{\sqrt{3}}{2} & -\frac{\sqrt{3}}{2} \\ 1 & 1 & 1 \end{bmatrix} \begin{bmatrix} a_1 \\ a_2 \\ a_3 \end{bmatrix} = \begin{bmatrix} \frac{x}{L} \\ \frac{y}{L} \\ \frac{\theta}{n} \end{bmatrix}
\tag{2.35}$$



The column vector a_1, a_2, a_3 can be solved.

$$\begin{bmatrix} a_1 \\ a_2 \\ a_3 \end{bmatrix} = \begin{bmatrix} \frac{2}{3} & 0 & \frac{1}{3} \\ -\frac{1}{3} & \frac{\sqrt{3}}{3} & \frac{1}{3} \\ -\frac{1}{3} & -\frac{\sqrt{3}}{3} & \frac{1}{3} \end{bmatrix} \begin{bmatrix} \frac{x}{L} \\ \frac{y}{L} \\ \frac{\theta}{n} \end{bmatrix}
\tag{2.35}$$

By the matrix, we can know any kind of movement just inputting into right column vector. For example: we want pure X direction movement, the ratio between x , y and θ is 1:0:0. That is:

$$\begin{bmatrix} a_1 \\ a_2 \\ a_3 \end{bmatrix} = \begin{bmatrix} \frac{2}{3} & 0 & \frac{1}{3} \\ -\frac{1}{3} & \frac{\sqrt{3}}{3} & \frac{1}{3} \\ -\frac{1}{3} & -\frac{\sqrt{3}}{3} & \frac{1}{3} \end{bmatrix} \begin{bmatrix} 1 \\ 0 \\ 0 \end{bmatrix} = \begin{bmatrix} \frac{2}{3} \\ -\frac{1}{3} \\ -\frac{1}{3} \end{bmatrix}$$

We know that $a_1 : a_2 : a_3 = 2 : -1 : -1$. The negative sign means different direction. Similarly, we can find how to composite the pure y direction and pure θ rotation. Table 2.1 lists the movement versus input. But the results are building on the linear hypothesis. We should proof that by simulation and experiment.

2.3.3 The simulation of 2-D Model

Because of the equipment for planar displacement measuring is too expensive to buy. We can not measure the 2-D experimental data exactly but roughly so far. Some of the simulation parameter such as frictional coefficient and damper coefficient are measured as the result of 1-D. The simulations of the mass-damper-spring model of 2-D IDM are also by Simulink. The block diagram of the 2-D IDM is shown as Figure 2.14(a). The block diagram of equation about X-axis is shown as Figure 2.14(b). The diagram consist of three parts included three inputs in one subsystem, three dynamics equations in three subsystems, three constraint equations in three subsystems. This method of connection will cause a problem which is algebraic loop. It can solve the problem by using Runge-Kutta method and setting the step size very small. The parameters of simulation are shown in table 2.2. The results of simulation are shown as Figure 2.15

to Figure 2.17. The results are match to our hypothesis of chapter 2.3.2. Although the equations is very complicating and difficult, but the assumptions by intuitions are correct.



Chapter 3 Experiment and Data Acquisition

3.1 One-Dimensional Experiment

3.1.1 Input and Measuring System

Figure 3.1 show the sketch of the 1-D IDM. Figure 3.2 and Figure 3.3 depict the overall structure and configuration with actual instrument for measuring the displacement of the piezoelectric actuator respectively. The photograph of the system and IDM are also presented in Figure 3.4 and Figure 3.5 In the experiment, the HP10705A interferometer with 10nm(0.4 μ m) resolution and 3MHz maximum data update rate measures the actual displacement of IDM. The sampling time of the data is controlled by DSP module and then sent to HP10885A. The primary function of The HP10885A Axis board is to convert reference and measured signals from a HP5517C laser head and measurement receiver to a 32-bit digital position word. The unit of measurement associated with the position word is a fraction of the wavelength of the laser light being used. A conversion is required if the position must be known in some other units such as mm, inch, etc.

After conversion, the raw data is read by DSP module directly. The main function of the DSP module are :

- (1) To send signals to HP10885A to control the sequence of data sample and hold (8 bits digital output) ;
- (2) To do data reading (32 bits digital input) ;
- (3) To produce driving voltage waveforms needed in the experiment (8 bits DA) and send to IDM.

We achieve this goal by utilizing code composer studio (CCS) software to integrate these tasks into a program which can be loaded to DSP controller. Because of low driving voltage waveforms from DSP module (8 bits DA), a voltage amplifier is needed to amplify the analog signal from 0~2V to 0~100V to drive the piezoelectric actuator. Table 3.1 lists the specifications of the piezoelectric actuator which we used.

3.1.2 DSP Program Flowchart

The 2407A DSP controllers shown in Figure 3.6 are designed to meet the needs of control-based applications. By integrating the high performance of a DSP core and the on-chip peripherals of a microcontroller into a single-chip solution, the 240xA series yields a device that is an affordable alternative to traditional microcontroller units (MCUs) and expensive multi-chip designs. At 40 million instructions per second (MIPS), the 2407A DSP controllers offer significant performance over traditional 16-bit microcontrollers and microprocessors. The 16-bit, low power, fixed-point DSP core of the 2407A device provides analog designers a digital solution that does not sacrifice the precision and performance of their systems. See details in Figure 3.7.

Code composer studio (CCS) is a fully software integrated development environment (IDE) for building and debugging programs for the DSK (DSP Starter Kit), i.e. the DSP board. CCS integrates all host and target tools in a unified environment to simplify DSP system configuration and application design. This easy to use development environment allows DSP designers of all experience levels full access to all phases of the code development process. The software is used for

three phases in the overall DSP system design process:

(1) Coding and building: writing code using the editor, creating a 'project', and compiling and linking.

(2) Debugging: syntax checking, probe points, break points

(3) Analysis: statistics, benchmarking, real-time debugging

Figure 3.8 describes the complete flowchart of the DSP program.

The processes are as follows:

(1) Start: The program starts.

(2) CPU will be initialized first. Then we set and enable time interrupt to define the sampling time.

(3) A while loop for DA control waveforms applying to the piezoelectric actuator is executed. The program waits for the time interrupt every 50 us (sampling rate = 20kHz).

(4) The program gets into time interrupt, the DSP module starts to read data by 32bits digital input.

(5) MSB Check: Because we do not know if an error occurs, the received data has to be checked first if an error occurs. The method provided from operating manual is to examine the most significant bit (MSB). If the MSB is one (true), it implies the data is correct. Otherwise, there exists an error. We should adjust all the experiments of the laser interferometer and see if the light status is ready especially the indicator of the receiver. Then restart the program again to step (1).

(6) Sign Check: The meaning of the second MSB indicates the sign of the position value; therefore it is sometimes called the sign bit. The sign bit zero (false) means positive and one (true) means negative position. Negative position needs to be calculated by 2's complement.

The position register is saved to the buffer.

(7) End: The program ends.

(8) Measurement: After the program ends, the position register saved in the buffer can be transferred to the real world displacement. The following equation describes how position is calculated from the value in the position register:

$$Position = Position\ register \times \frac{\lambda}{N} \times Compensation\ number$$

where:

$\lambda = 632.99135$ nanometers (for HP5517C)

$N = 64$ when linear optics being used

$N = 128$ when plane mirror optics being used

$N = 256$ when high resolution optics being used

$$Compensation\ number = \frac{1}{Air's\ index\ of\ refraction} = 0.9997288$$

Then the experimental results will be plotted into a time-position graph step by step continuously. These files can help us to compare the results of different driving waveforms.

3.1.3 The Results of One-Dimensional Experiment

Figure 3.9 shows the position versus time of slider. We compare with Figure 2.11 which is the simulation result. Experiment and simulation are matching. The step size about experiment is about $0.694 \mu\text{m}$. The step size about simulation is about $0.677 \mu\text{m}$. There is only 2.4% error between experiment and simulation. But there are some phenomenons to deserve to be mentioned. The forward movement of one-dimension

IDM is similar to the backward movement but little difference in step size. One possibility is to assume the friction between the bottom of one-dimension IDM and the surface of the guide in forward and backward is quite different since the inaccurate manufacture of IDM. Another possibility may be the characteristics of piezoelectric actuator. The housing PZT actuators can only extension but contraction. There is a spring inside the house of the PZT pulling the piezo stack to the original length. Because of the difference between the forward and backward movement of the one-dimension IDM, we should know the degree of the difference. Base on the condition of manufacture, two piezoelectric actuators applied the same voltage waveform cannot produce the same movement.



3.2 Two-Dimensional Experiment

3.2.1 Input and Measuring of 2-D System

Figure 3.10 shows the experimental flowchart. Figure 3.11 to figure 3.14 are pictures of the experiment apparatus and scenario. The AD/DA board generates the asymmetric triangle wave by board PCI-6711. The detail attribute of experimental apparatus are shown in Table 3.2. The board and PC are commuting by software “NI LabView Signal Express”. We just input what waveform we want into Signal Express, the wave will generated by this board. Every triangle wave is established by 500 points. There are two kinds of waveforms in the experiments shown in figure 3.15. Figure 3.15(a) shows forward movement waveform. The left segment of wave form Point 1 to point 475 is uphill from zero to

maximum uniformly. Point 476 to point 500 is downhill from maximum to zero uniformly. The duty of asymmetric triangle wave is fixing at 95%. Figure 3.15(b) is opposite situation that making the mechanism moving backward. The amplitude of waveform is adjusting by power amplifier. However, the maximum voltage generating by PCI-6711 is 5V. This is not enough to drive PZT that require 0~150V high voltage. We use Burleigh power amplifier to enlarge the original waveform from board. Adjust the waveform to 80V. According to the introduction of PZT, the maximum elongation of PZT will keeping at $8 \mu\text{m}$ if input voltage is 80V. Because of the movement are so small to observe, we observe the mechanism via “Olympus BX51M” microscope. We can observe the motion about $1 \mu\text{m}$. Figure 3.16 is the picture shot via microscope. The grid in picture is standard calibration scale. The pitch every grid is $10 \mu\text{m}$. We record the movement by high speed camera “X-stream XS-4”. Although the maximum frame rate of high speed camera is 5140fps, but restricting by light. The maximum frame rate we test is 1000 fps. Figure 3.17 is the picture high speed camera shoot. We can recognize the coordinate in the picture and analysis the trajectory IDM moved.

3.2.2 The Results of Two-Dimensional Experiment

Figure 3.15 to figure 3.17 show the results of 2-D experiment. Figure 3.15 is pure X-direction translation. The step size is about $0.3243 \mu\text{m}$. Figure 3.16 is pure Y-directions translation. The step size is about $0.5379 \mu\text{m}$. Figure 3.17 is pure rotation. The step size is about 0.0022378° . The

movement trajectory is similar between simulation and experiment. The IDM movement is like straight line by naked eye. But we find the trajectory is including not only forward movement but also small size of backward movement instead of straight via high speed camera. But there is some error about step size, especially in rotation. Table 3.3 lists the comparison between simulation and experiment. The rotation step size of experiment is larger than simulation.



Chapter 4 Conclusion

We found that the 2-D IDM can be realized to achieve the purpose of precise positioning. According to the results of simulations and experiments, the movement of 2-D IDM can be controlled by us and it can be predicted. It help us to develop this mechanism for precise positioning. The 2-D IDM dynamic equations have be revised. In this research, but the change of results are not obvious. One possibility is the angular speed is very small that can be neglect. Here we have some conclusion as below.

- (1) The applied voltage increases, the IDM will move and rotate faster.
- (2) A new explanation about the IDM motion by pulse hypothesis is be done completely
- (3) The static friction force is not important in the process of IDM moving.

There are some problem in this experiment included how to estimate parameters of system, the frictional coefficient especially. The other problem is the cable of the actuator. When the IDM is moving, the cable which get stuck produce force to push or pull the mechanism. The only way to solve this problem is to reduce the radius of the cable. It can reduce the weight and affection of the cable. Measure is the most important problem because the pixels of digital camera are limited. This measuring system cannot help us to obtain more accurate data. It needs more accurate image process system to obtain image data and to calculate the movement of the 2-D IDM. There is one problem occurred. The

contact between the plate and the surface is not close, especially in the center of the plate.

The 2-D IDM will be developed to be more accurate and reliable by solving the above problems in the future.



Reference

- [1] S. Ling, H. Du & T. Jiang, “Analytical and Experimental Study on a Piezoelectric Linear Motor”, *Smart Materials and Structures*, Vol.7, No.3, Jun, 1998, pp.382-388.
- [2] T. Higuchi, Y. Yamagata, K. Furutani & K. Kudoh, “Precise Positioning Mechanism Utilizing Rapid Deformations of Piezoelectric Elements”, *Proceedings of the IEEE MEMS Workshop*, 1990, pp.222-226.
- [3] J. Mendes, M. Nishimura, K. Tomizawa, Y. Yamagata & T. Higuchi, “Print Board Positioning System Using Impact Drive Mechanism”, *Proceedings of the SICE Annual Conference*, Jul, 1996, Tottori, Jpn, pp.1123-1128.
- [4] K. Furutani, T. Higuchi, Y. Yamagata & N. Mohri, “Effect of Lubrication on Impact Drive Mechanism”, *Precision Engineering*, Vol.22, No.2, 1998, pp.78-86.
- [5] M. Kurisu, T. Yoshikawa, “Tracking Control for An Object in Pushing Operation”, *Proceedings of the 1996 IEEE/RSJ International Conference on Intelligent Robots and Systems*, Vol.2, Nov, 1996, Osaka, Jpn, pp.729-736.
- [6] Y. Wang, M. Mason, “Two-Dimensional Rigid-Body Collisions with Dry Friction”, *Transactions of the ASME*, Vol.59, Sep, 1992, pp.635-642.
- [7] Y. Yamagata, T. Higuchi, “A Micropositioning Device for Precision Automatic Assembly Using Impact Force of Piezoelectric Elements”, *Proceedings of IEEE International Conference on Robotics and*

- Automation*, May, 1995, Nagoya, Jpn, pp.666-671.
- [8] H. Alexander, H. Lakhani, “Robotic Control of Sliding Object Motion and Orientation”, *Proceedings of the 1996 IEEE/RSJ International Conference on Robotic and Automation*, Apr, 1996, Minneapolis, Minnesota, pp.3336-3342.
- [9] K. Furutani, N. Mohri & T. Higuchi, “Self-Running Type Electrical Discharge Machine Using Impact Drive Mechanism”, *Proceedings of IEEE/ASME International Conference on Advanced Intelligent Mechatronics*, Jun, 1997, Tokyo, Jpn, pp.88.
- [10] K. Furutani, N. Mohri & T. Higuchi, “Self-Running Type Electrical Discharge Machine Using Impact Drive Mechanism”, *Seimitsu Kogaku Kaishi/Journal of the Japan Society for Precision Engineering*, Vol.63, No.9, Sep, 1997, pp.1290-1294.
- [11] K. Ikuta, S. Aritomi & T. Kabashima, “Tiny Silent Linear Cybernetic Actuator Driven by Piezoelectric Device with Electromagnetic Clamp”, *Proceedings of the IEEE Micro Electro Mechanical Systems Workshop*, Feb, 1992, Travemuende, Ger, pp.232-237.
- [12] T. Idogaki, H. Kanayama, N. Ohya, H. Suzuki & T. Hattori, “Characteristics of the Piezoelectric Locomotive Mechanism for an In-Pipe Micro Inspection Machine”, *Proceeding of the International Symposium on Micro Machine and Human Science*, Oct, 1995, Nagoya, Jpn, pp.193-198.
- [13] 鄭仲哲, 「利用壓電致動器之精密定位」, 國立交通大學, 博士論文, 民國 92 年。
- [14] 陳立明, 「微步進機構定位之研究」, 國立交通大學, 碩士論文,

民國 94 年。

[15] 鄧明欣，「二維微步進機構定位之研究」，國立交通大學，碩士
論文，民國 96 年。

[16] Piezo Motor Solutions for Automation & Ultra-Precision Motion
Control ，「<http://piezo-motor.net/>」。

[17] 東京大學，Advanced Mechatronics Laboratory ，
「<http://www.aml.t.u-tokyo.ac.jp/main.html>」。



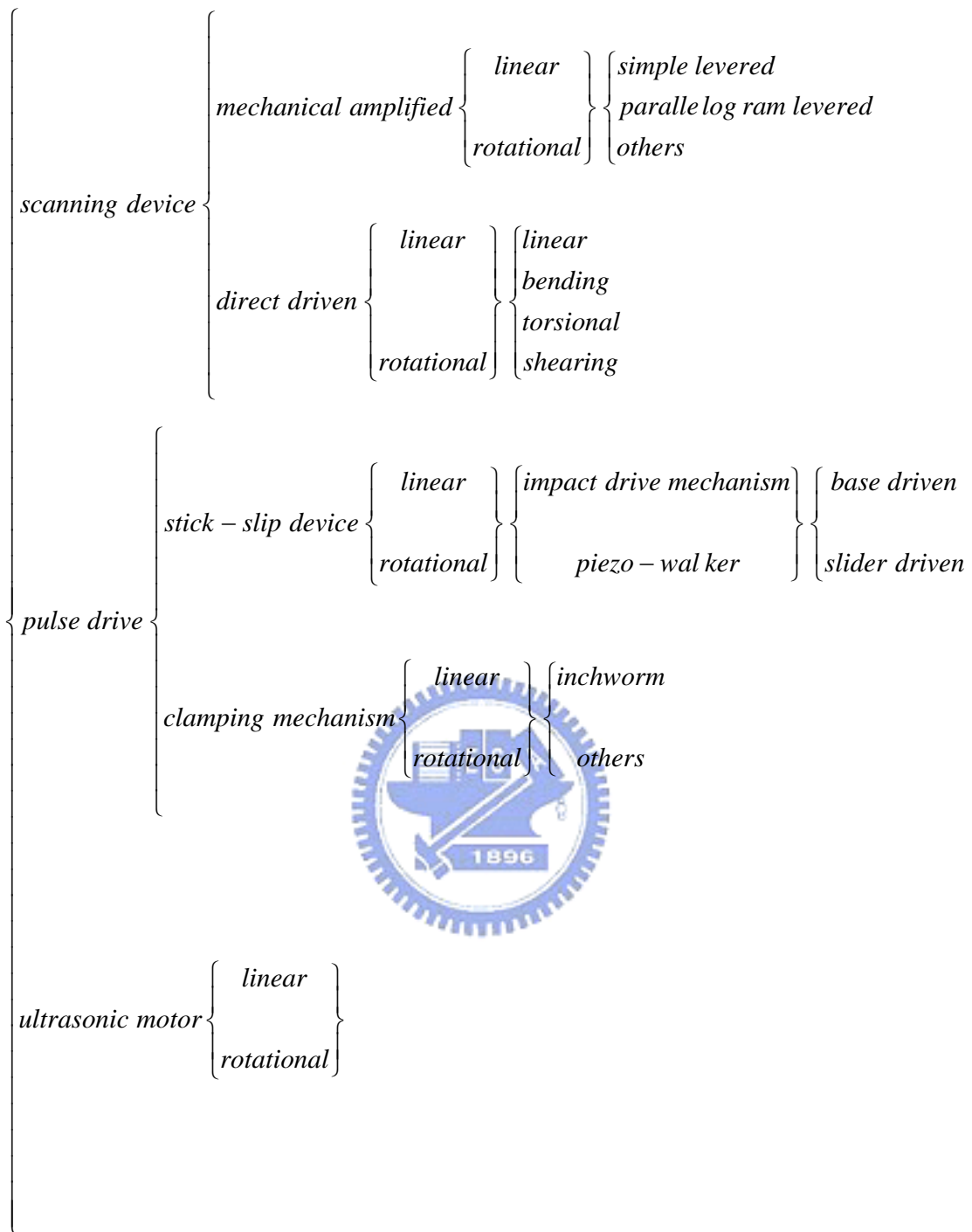


Figure 1.1 Classification of piezoelectric positioning device

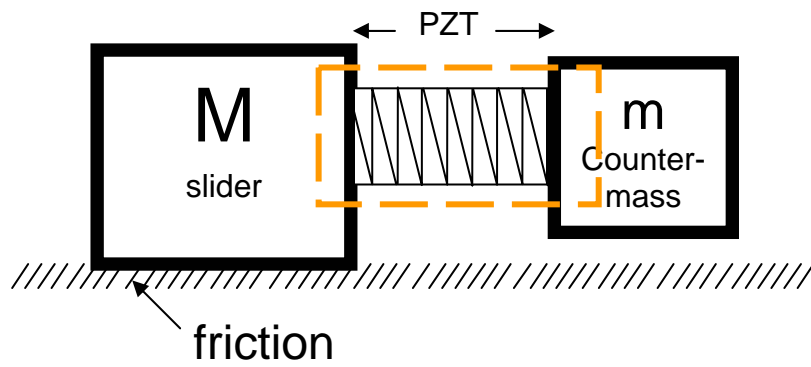


Figure 1.2 Sketch of 1-D mechanism.

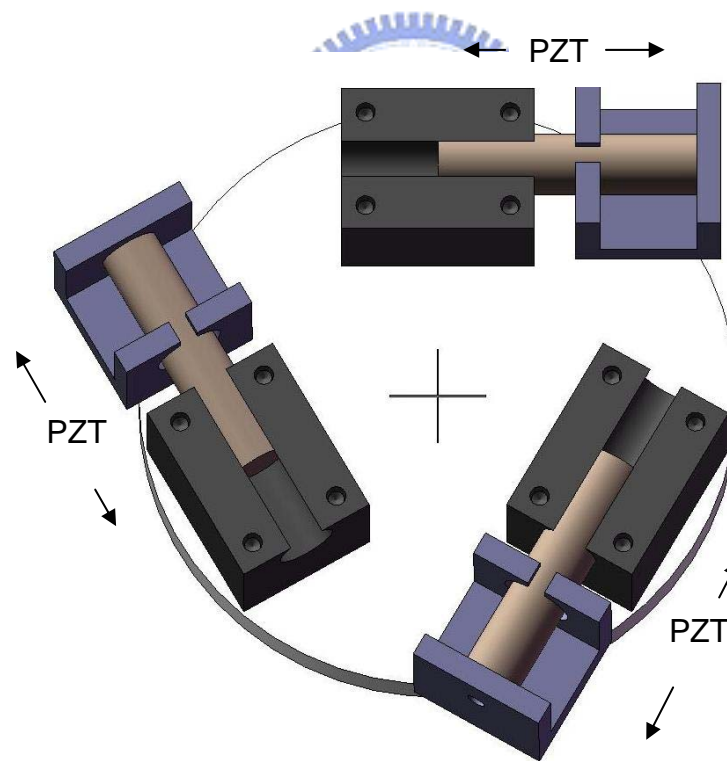
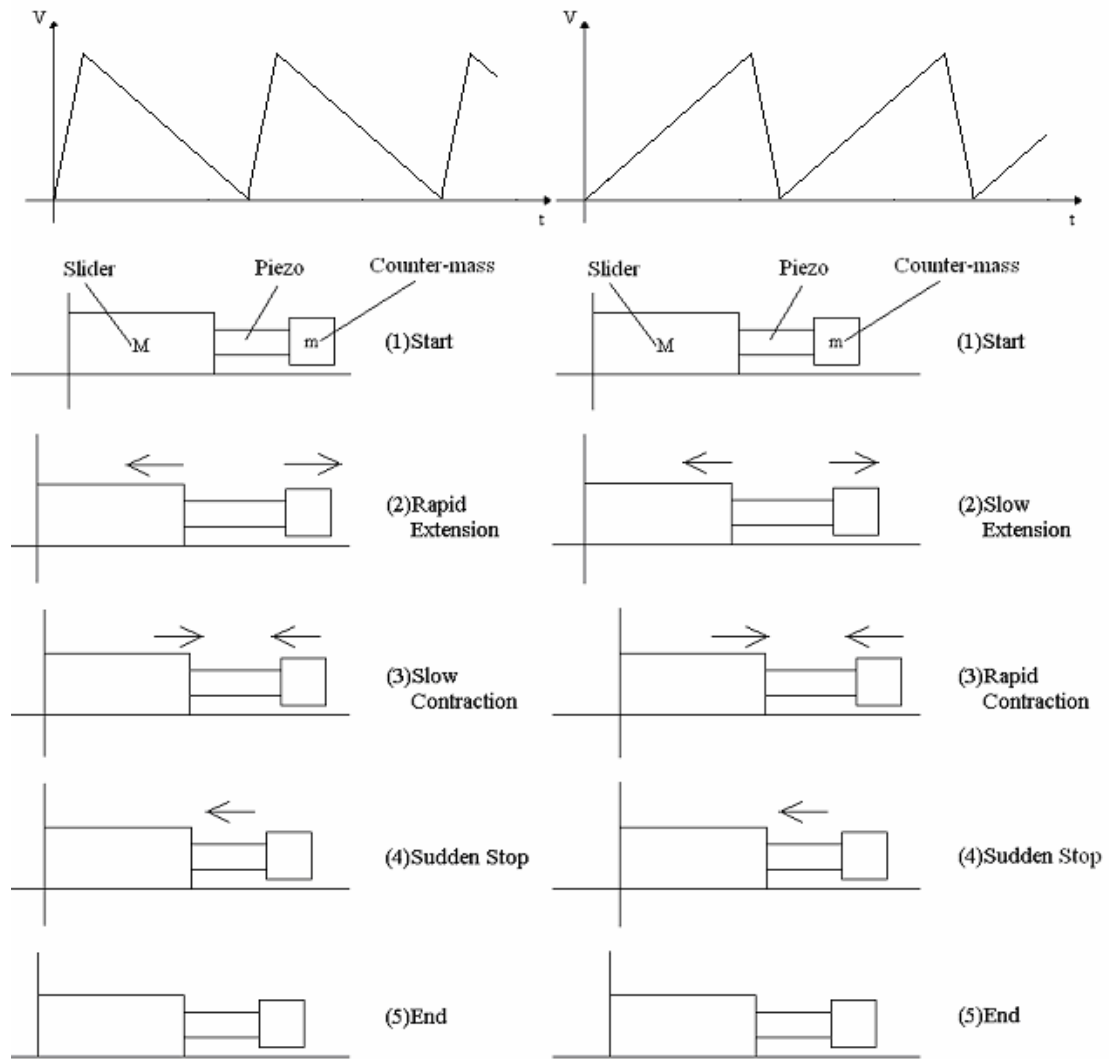


Figure 1.3 2-D and 3DOF mechanism sketching by Solidwork



(a) Backward movement

(b) Forward movement

Figure 2.1 Operating principle of IDM

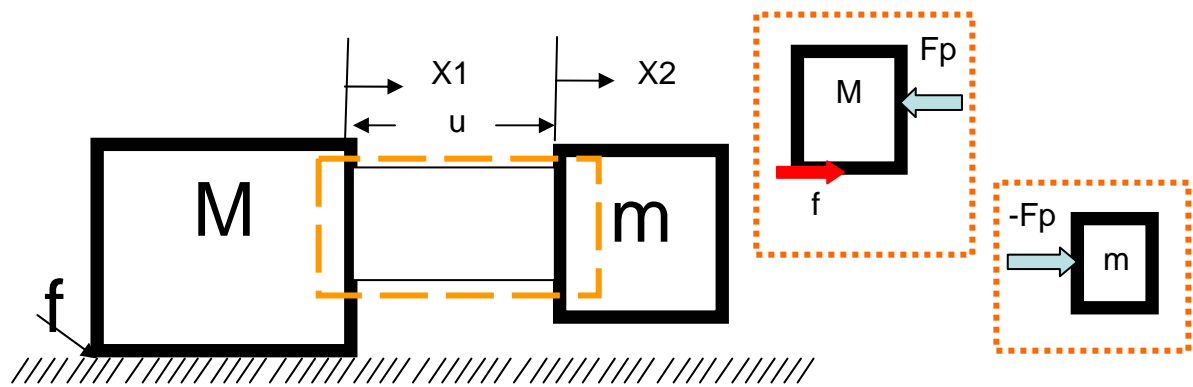


Figure 2.2 Rigid body model of 1-D IDM

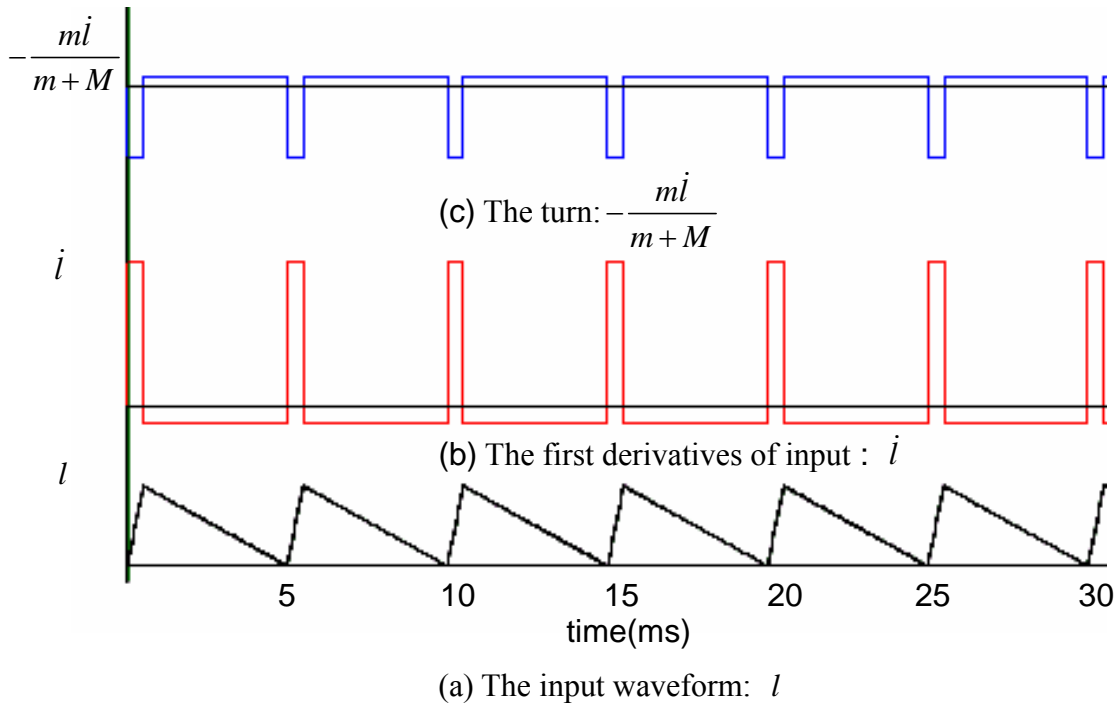


Figure 2.3 Asymmetric triangle input waveform

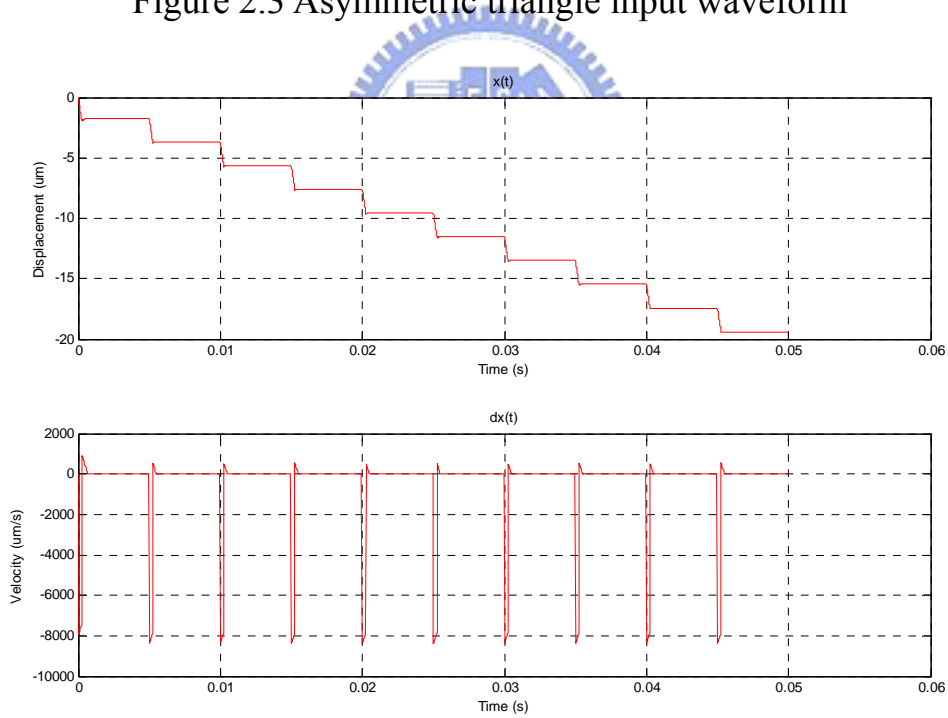


Figure 2.4 Simulation result of rigid body model

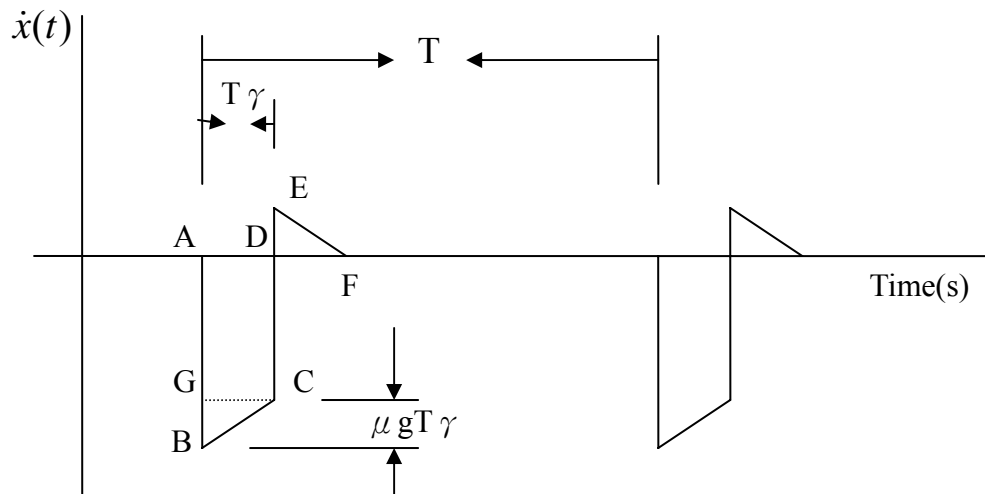


Figure 2.5 $\dot{x}(t)$ graph and step size analysis

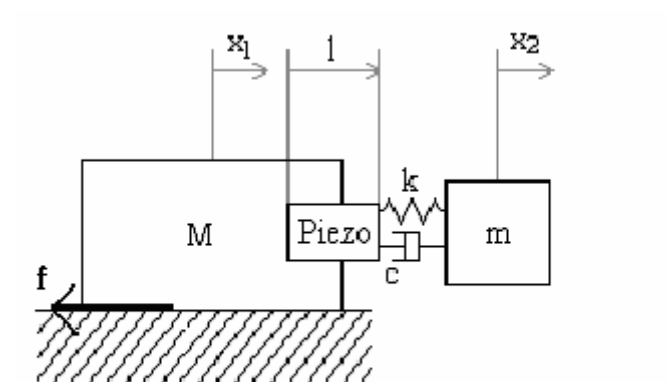


Figure 2.6 Mass-damper-spring model of 1-D IDM

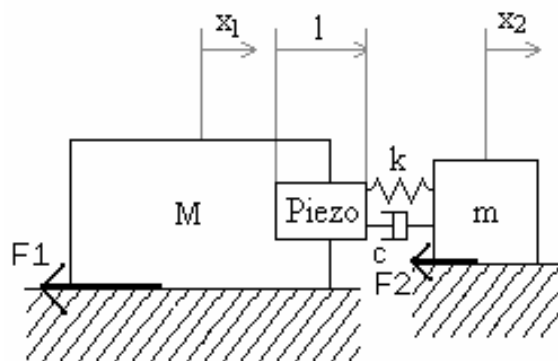


Figure 2.7 Mass-damper-spring model of 1-D IDM

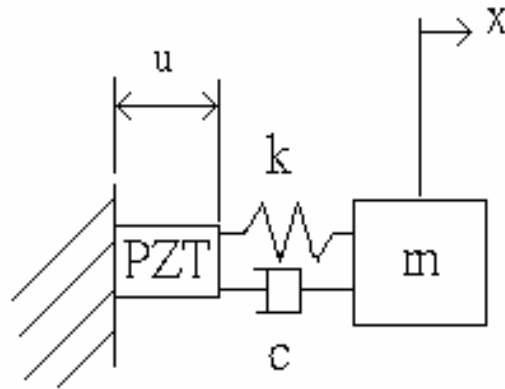


Figure 2.8 MCK model of system identification

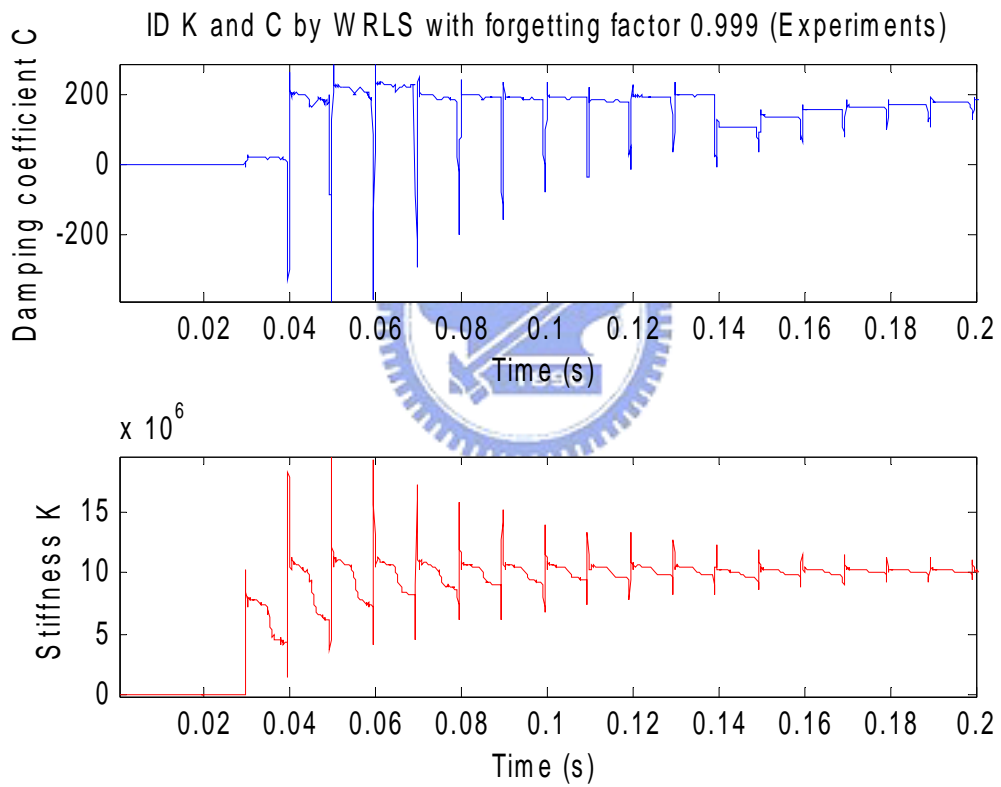


Figure 2.9 The result of estimation

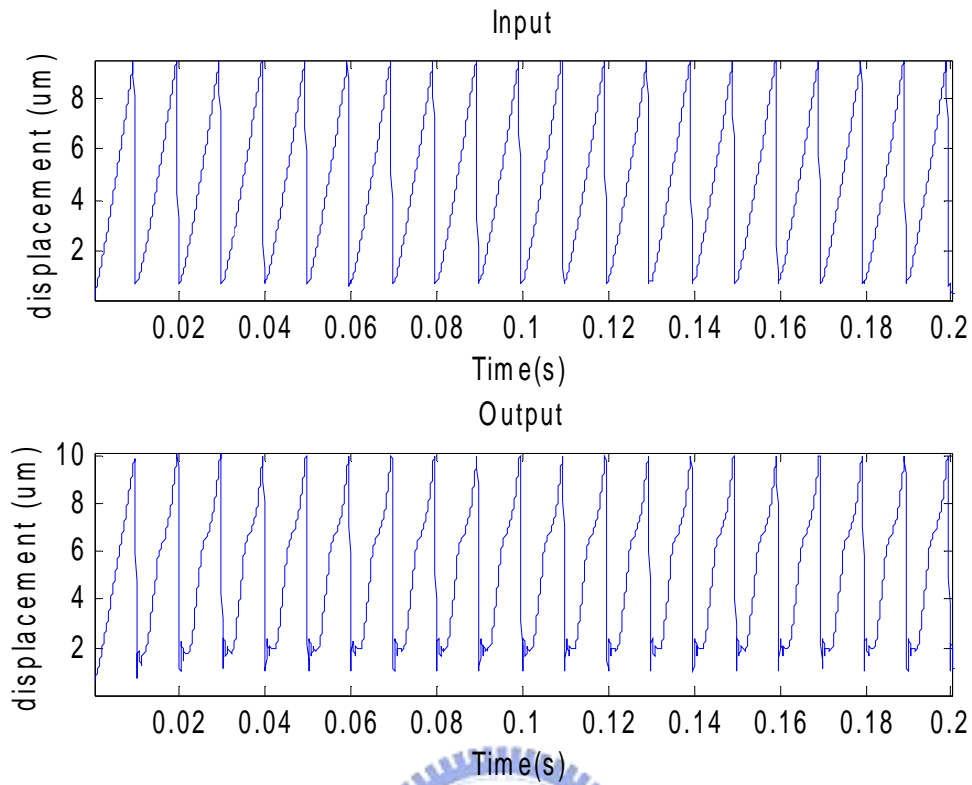


Figure 2.10 input and output of piezoelectric actuator

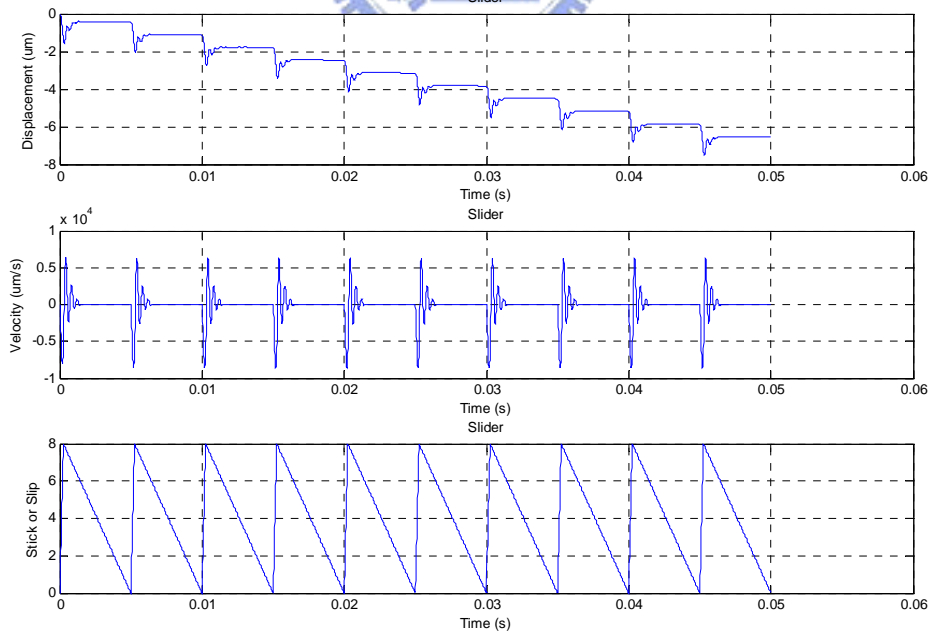


Figure 2.11 Displacement of 1-D IDM (80V, 200Hz, 95% duty)

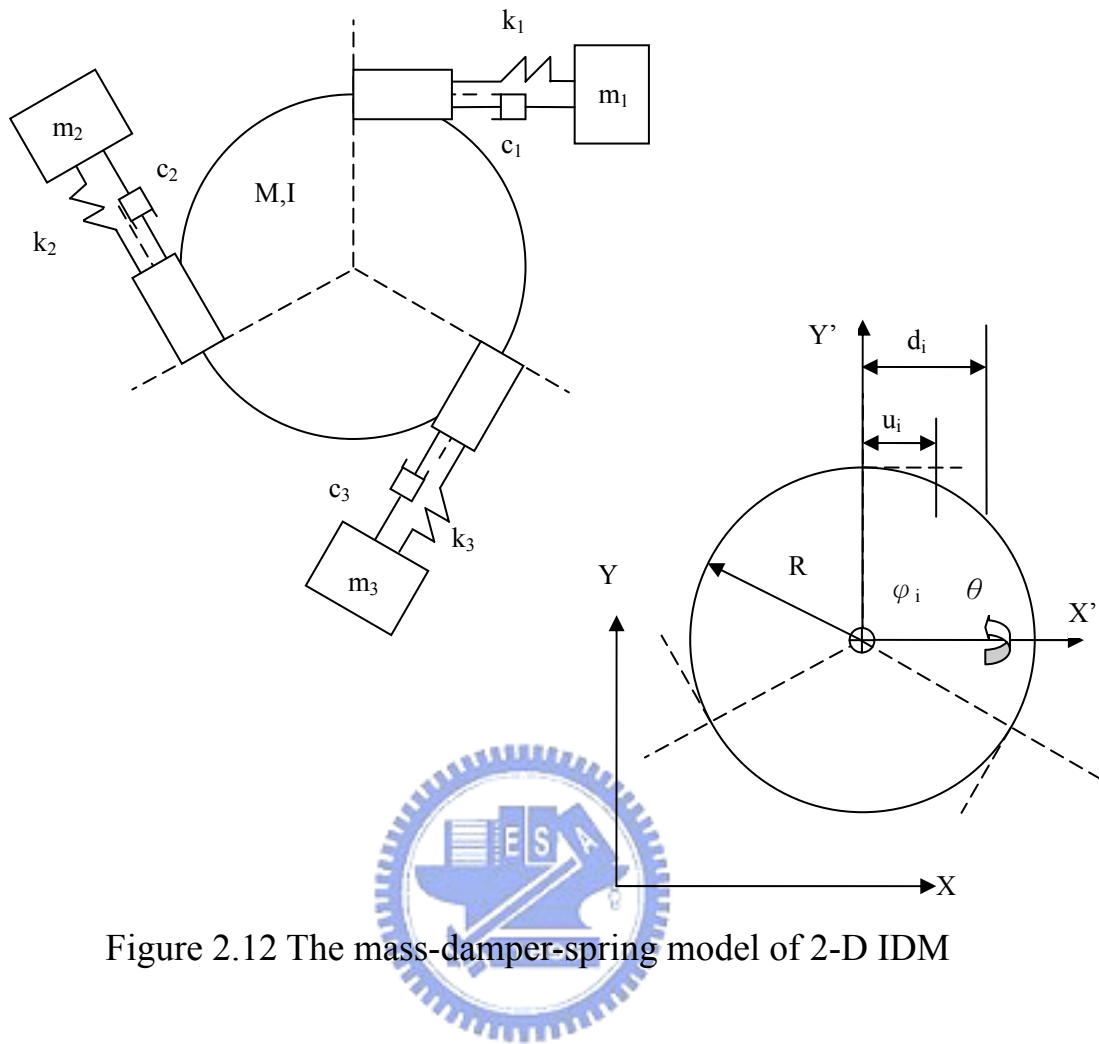


Figure 2.12 The mass-damper-spring model of 2-D IDM

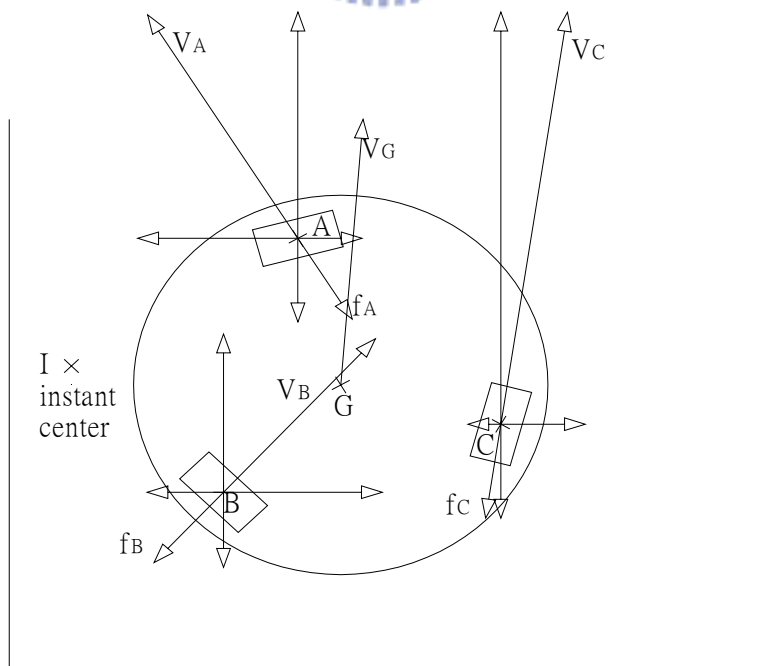


Figure 2.13 Velocity and friction force act at A,B,C points

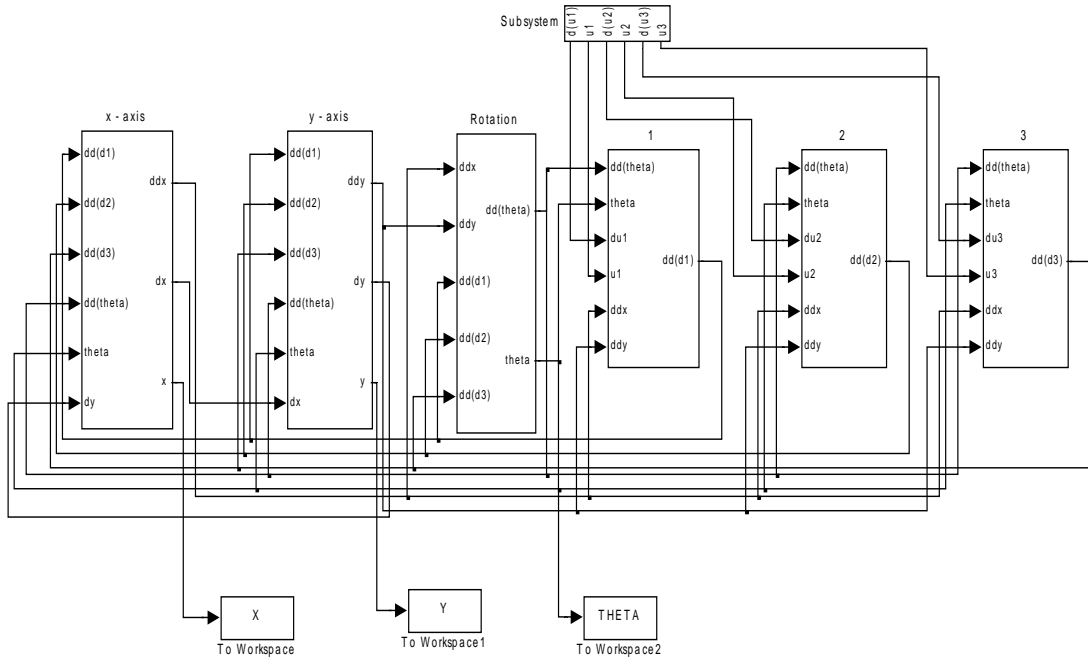


Figure 2.14(a) Block diagram over view of the model of 2-D IDM

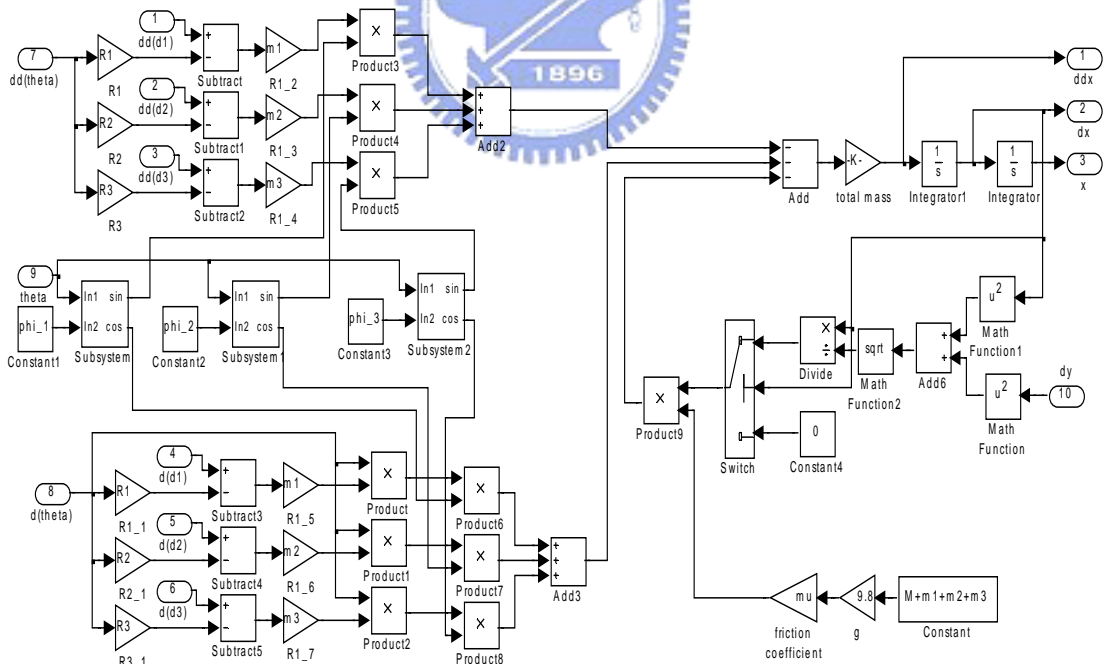


Figure 2.14(b) Block diagram of dynamic equation about X-axis

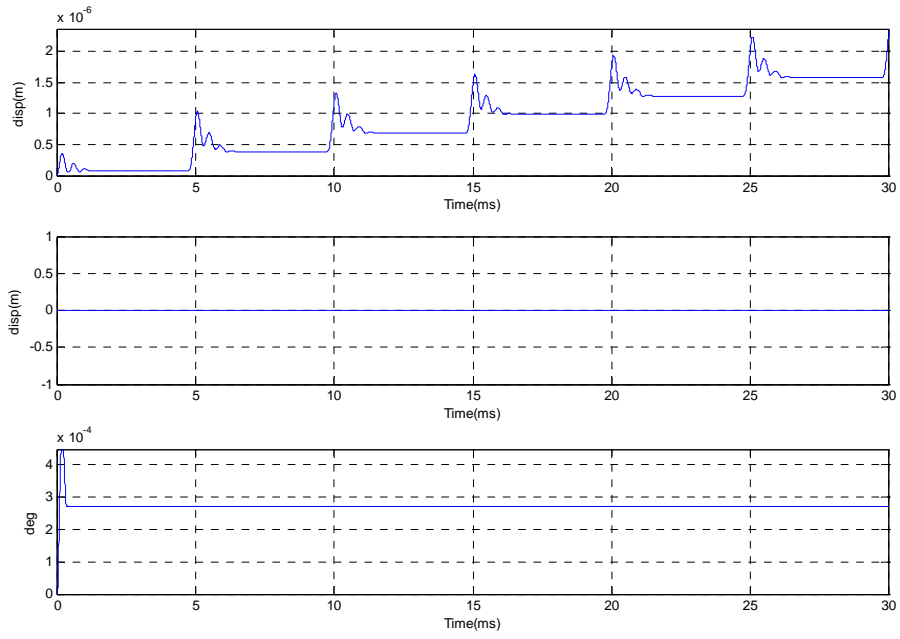


Figure 2.15(a) Displacement versus time
(Simulation results of pure X translation)

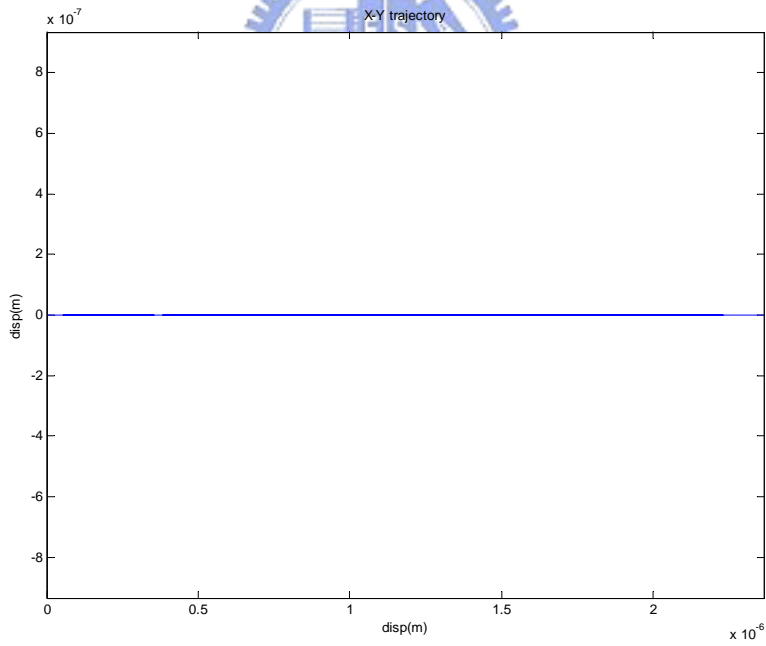


Figure 2.15(b) X-Y trajectory graph
(Simulation results of pure X translation)

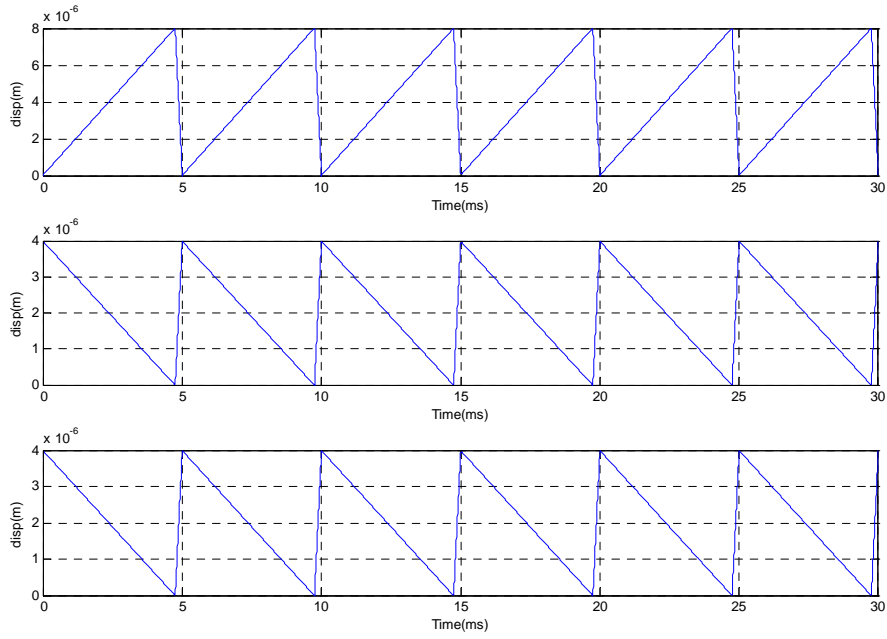


Figure 2.15(c) Input waveforms about 3 actuators
(Simulation results of pure X translation)

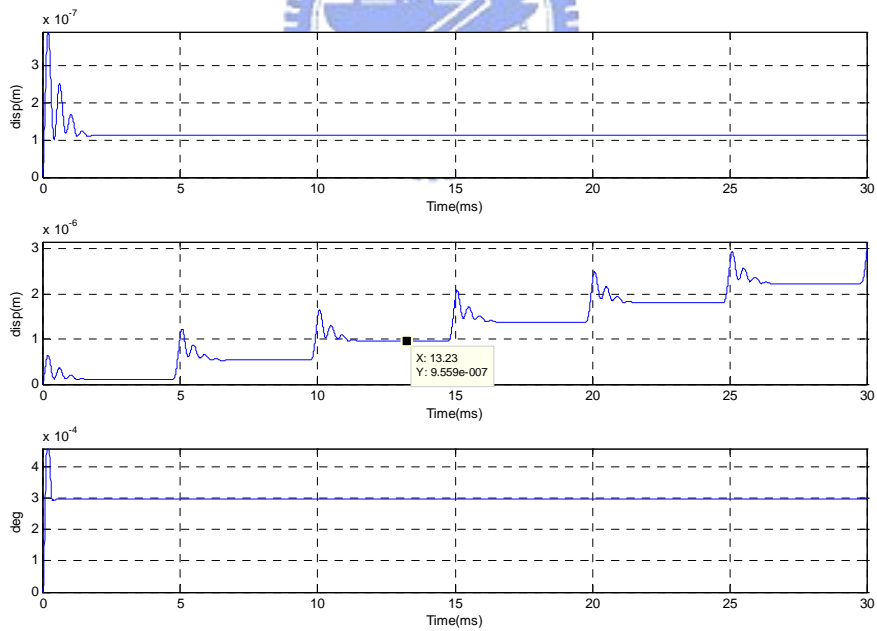


Figure 2.16(a) Displacement versus time
(Simulation results of pure Y translation)

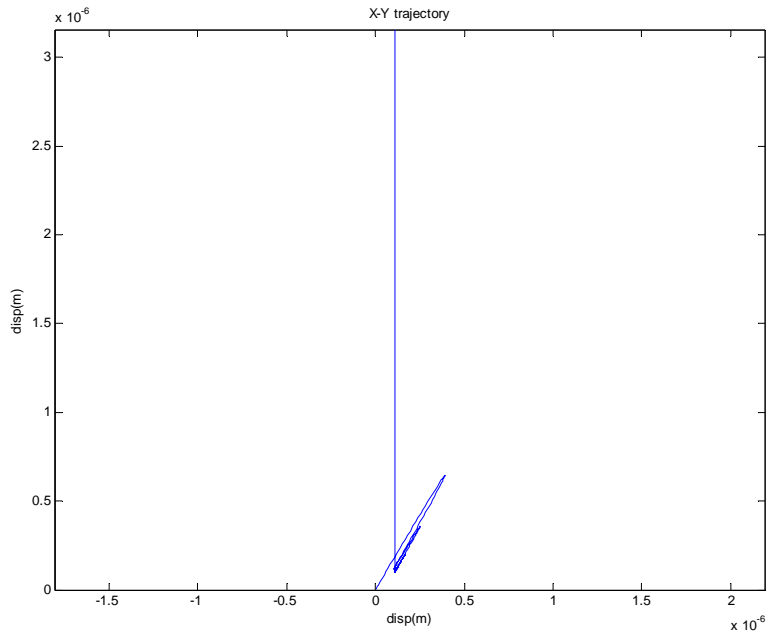


Figure 2.16(b) X-Y trajectory graph
(Simulation results of pure Y translation)

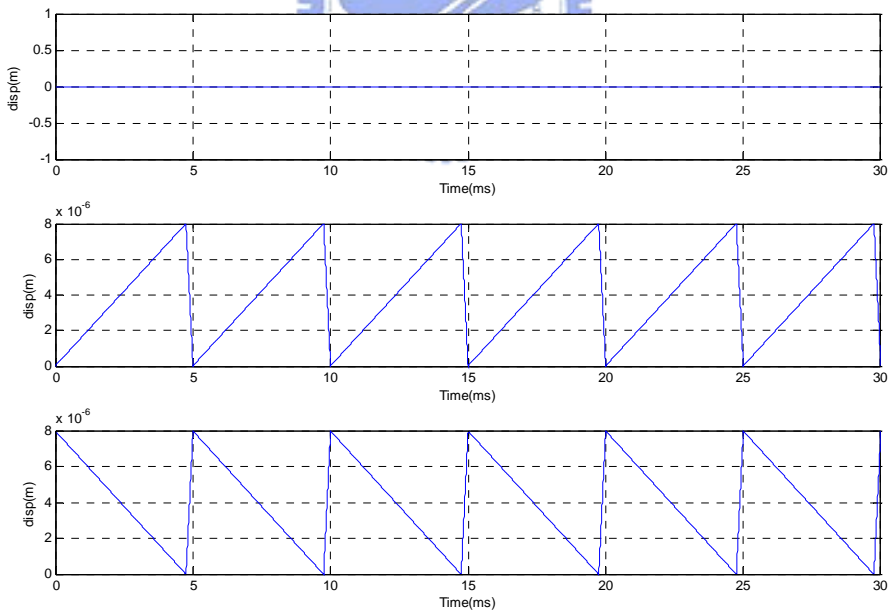


Figure 2.16(c) Input waveforms about 3 actuators
(Simulation results of pure Y translation)

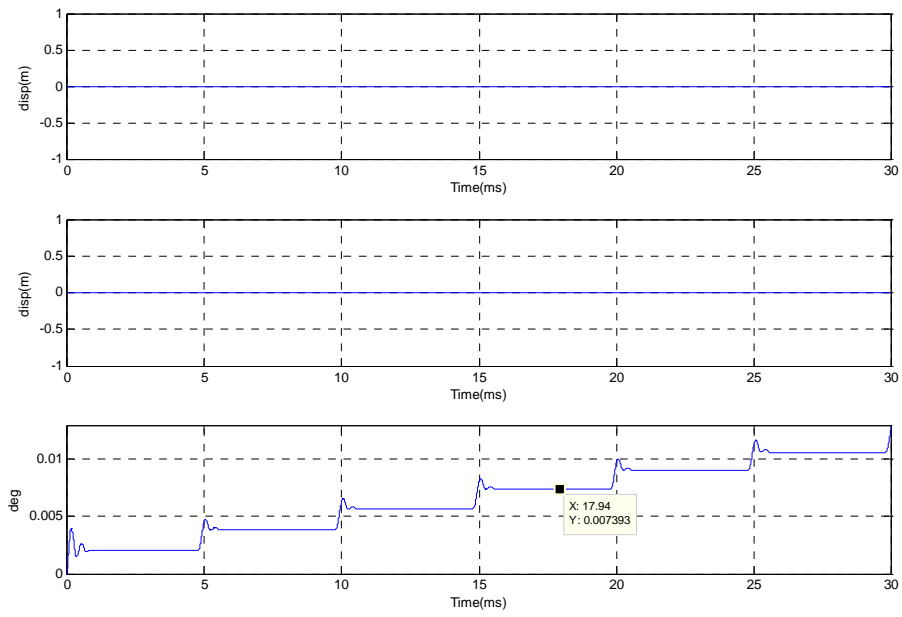


Figure 2.17(a) Displacement versus time
(Simulation results of pure rotation)

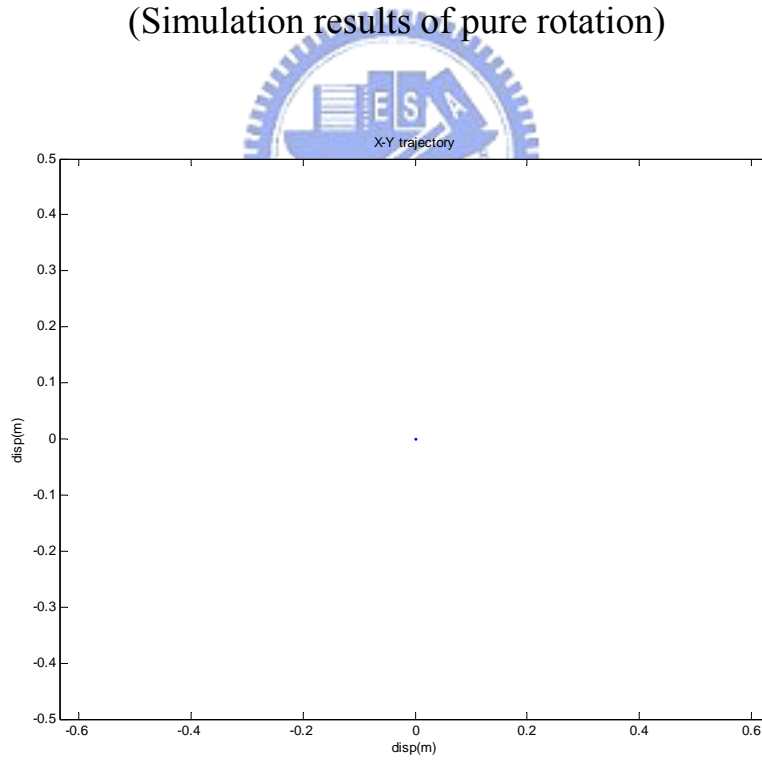


Figure 2.17(b) X-Y trajectory graph
(Simulation results of pure rotation)

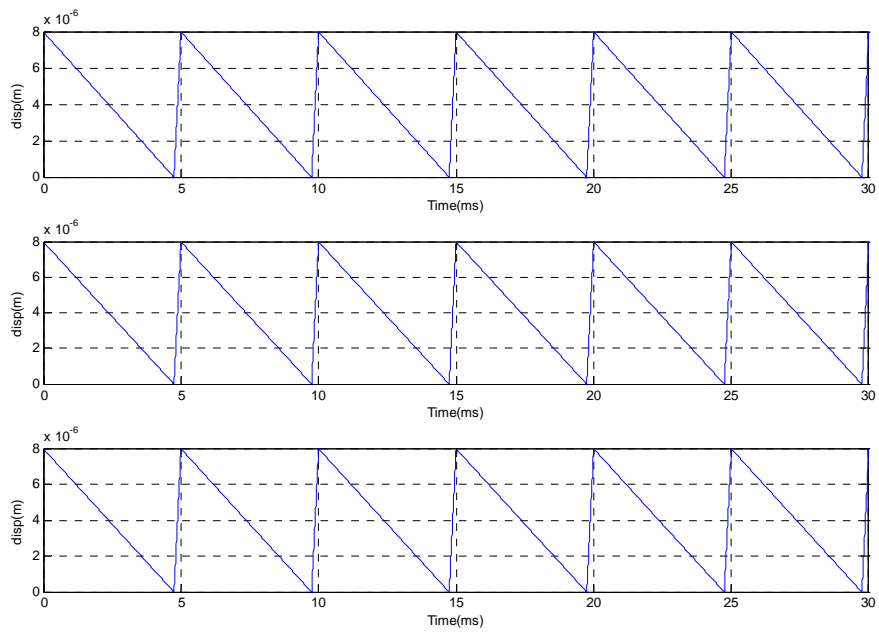


Figure 2.17(c) Input waveforms about 3 actuators
(Simulation results of pure rotation)

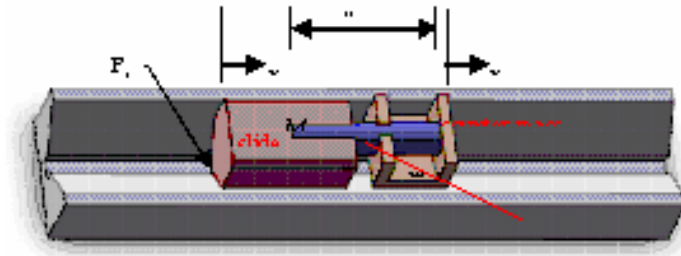


Figure 3.1 1DOF mechanism sketch

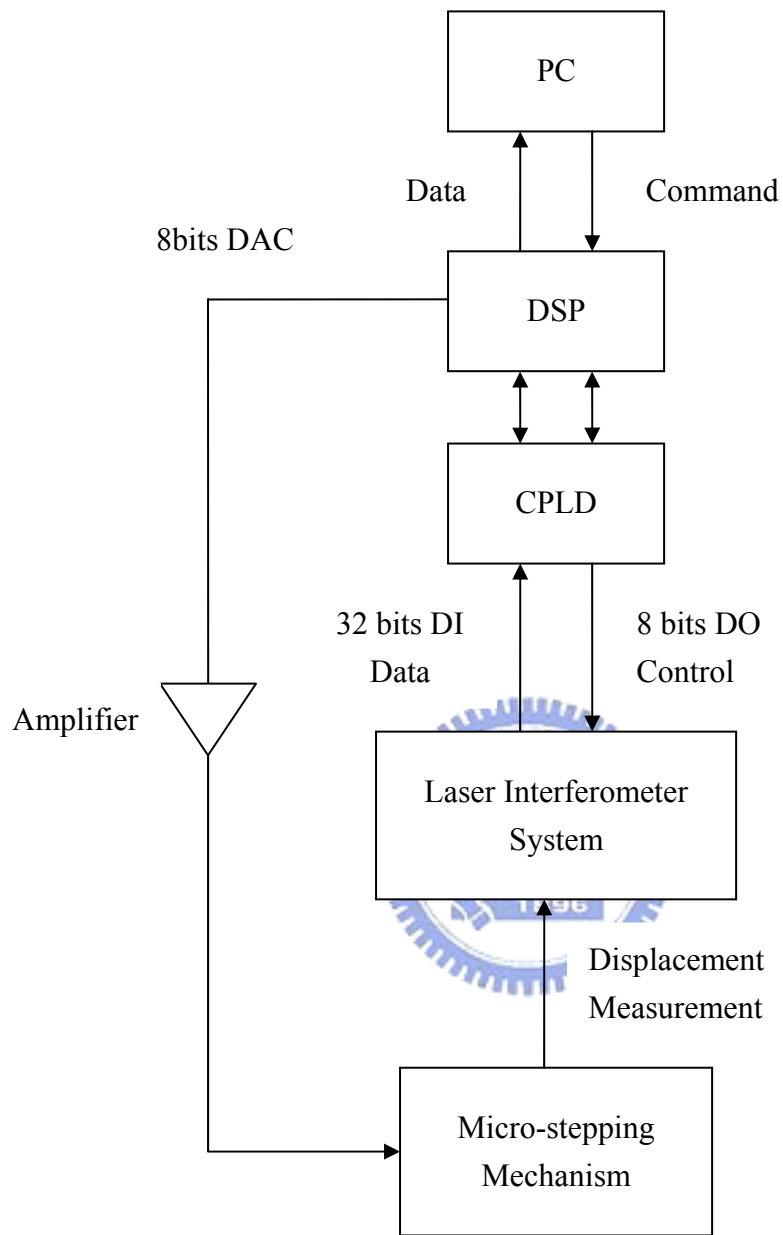


Figure 3.2 Structure for measurement for 1-D IDM

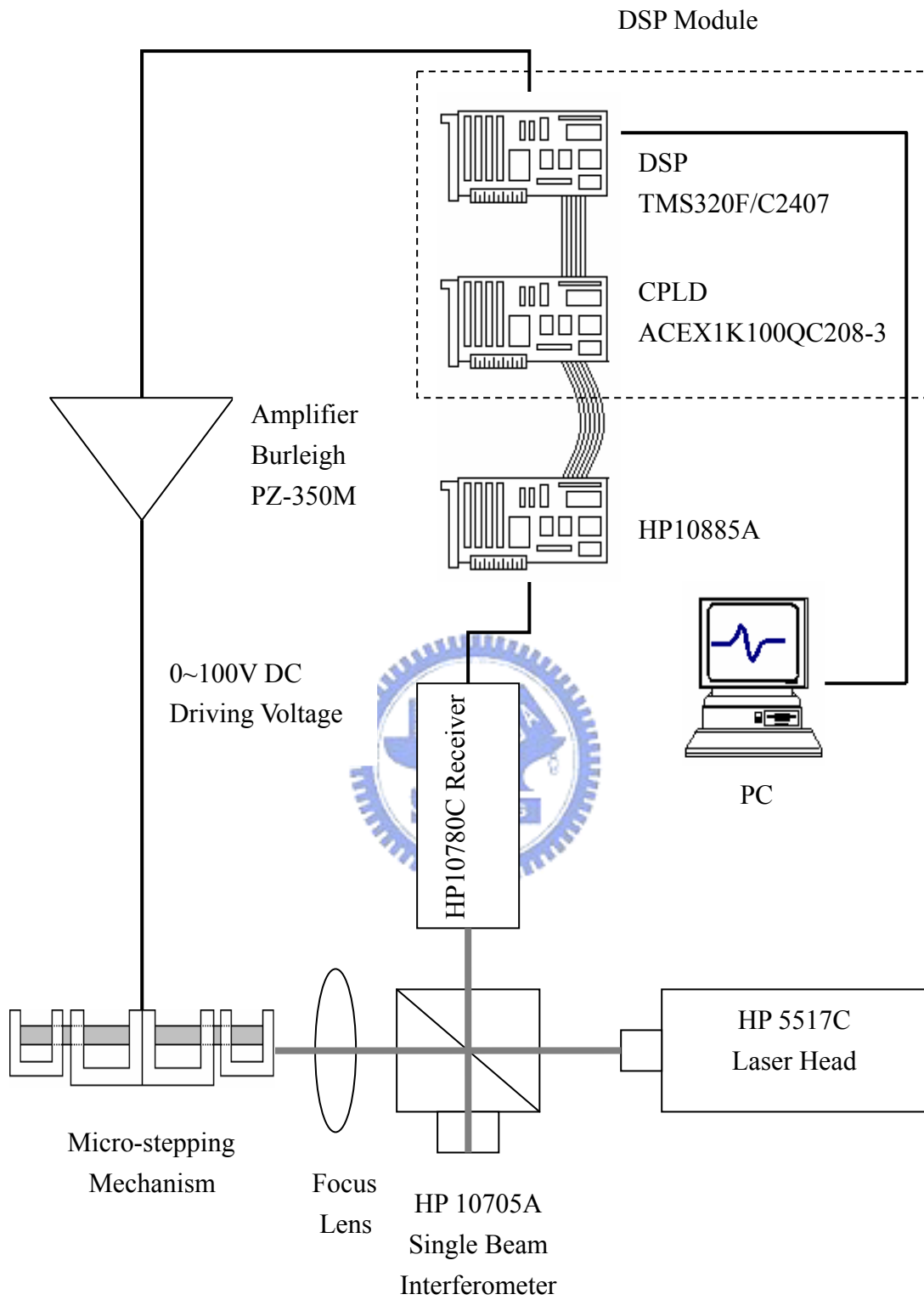


Figure 3.3 System configuration

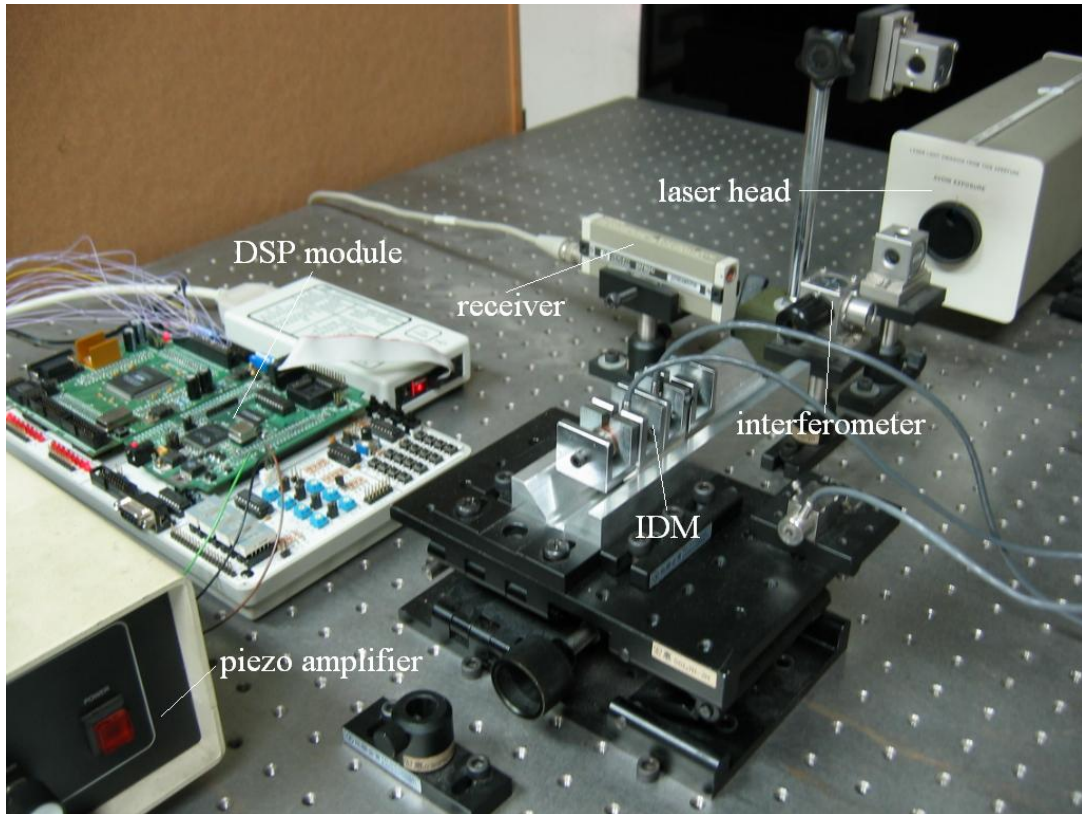


Figure 3.4 Experiment setup of 1-D IDM

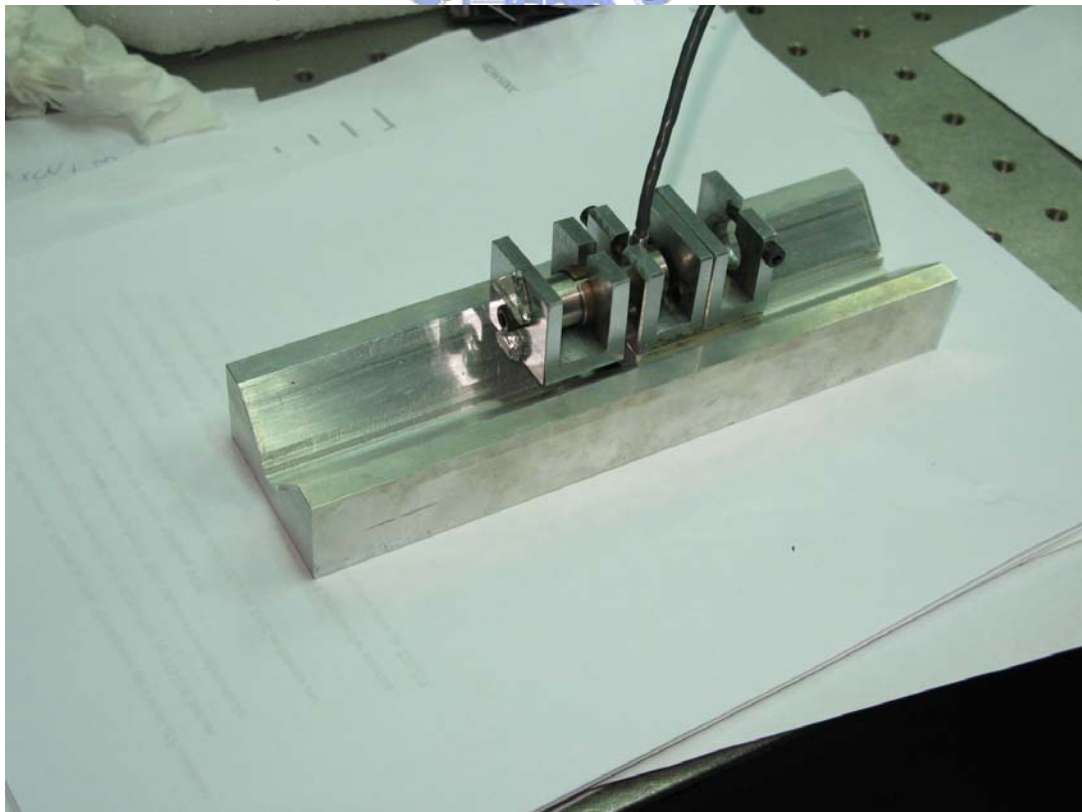


Figure 3.5 1-D Impact drive mechanism

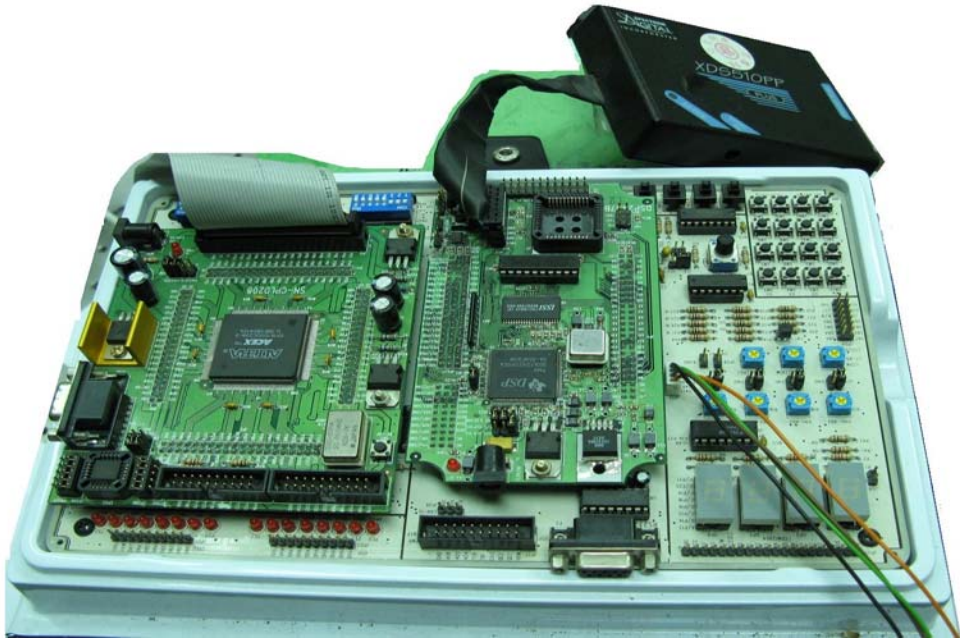


Figure 3.6 DSP module

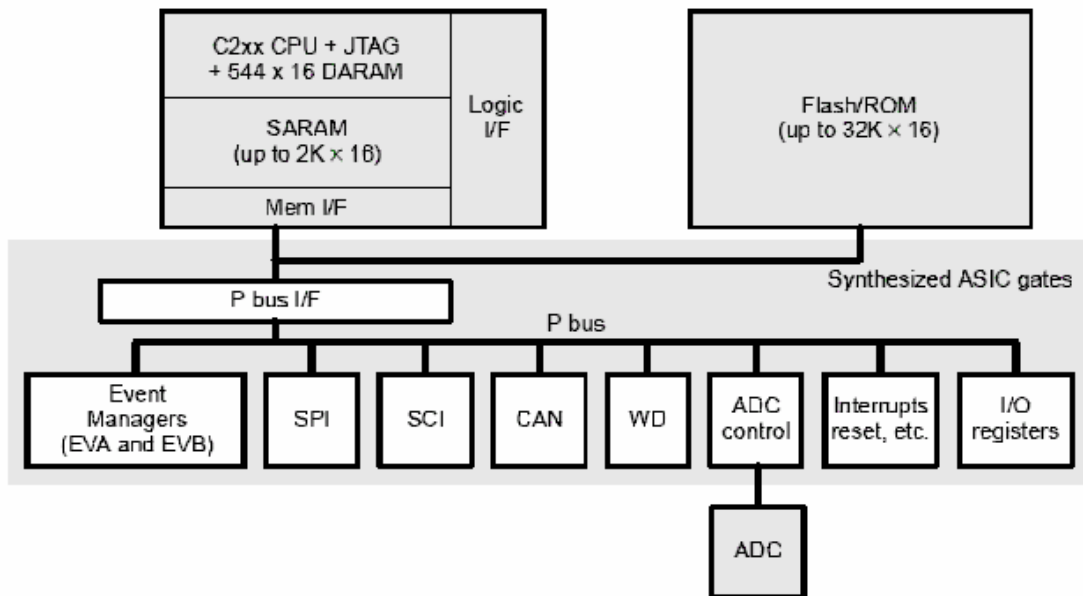


Figure 3.7 2407A device architecture

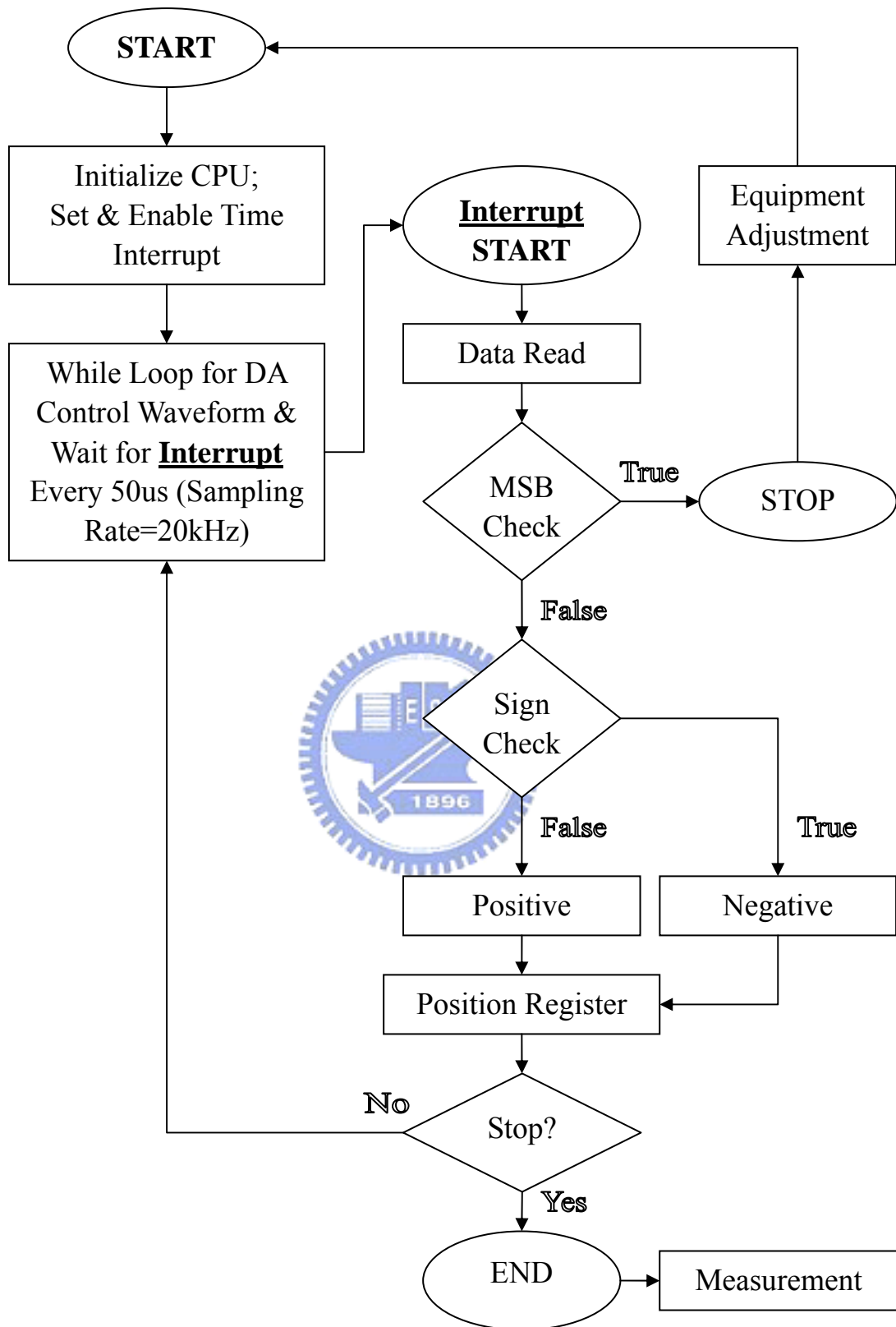


Figure 3.8 Program flow

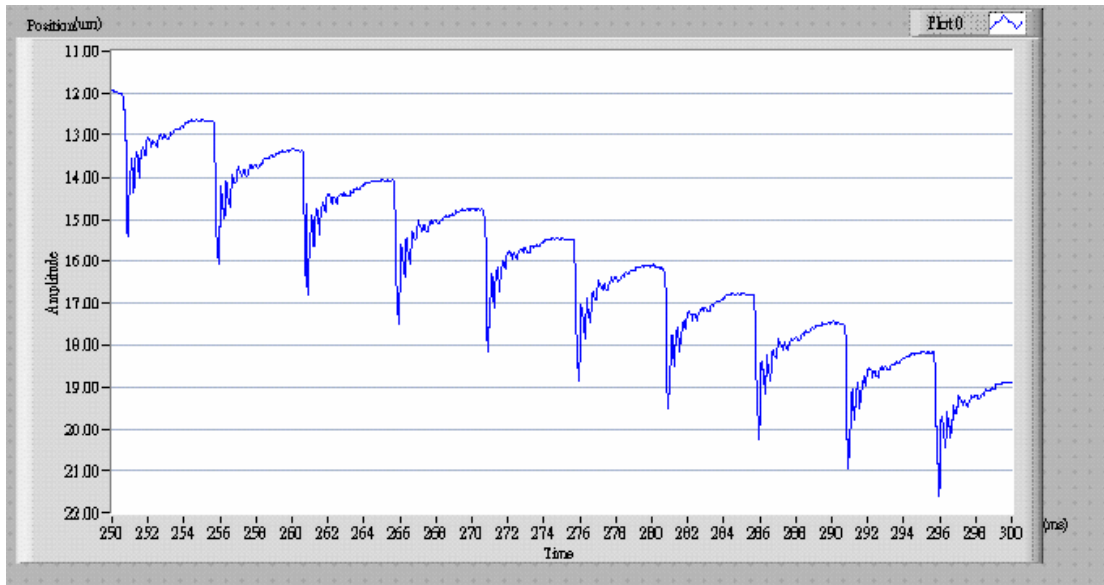


Figure 3.9 The results of 1-D experiment, 200Hz, 5% duty

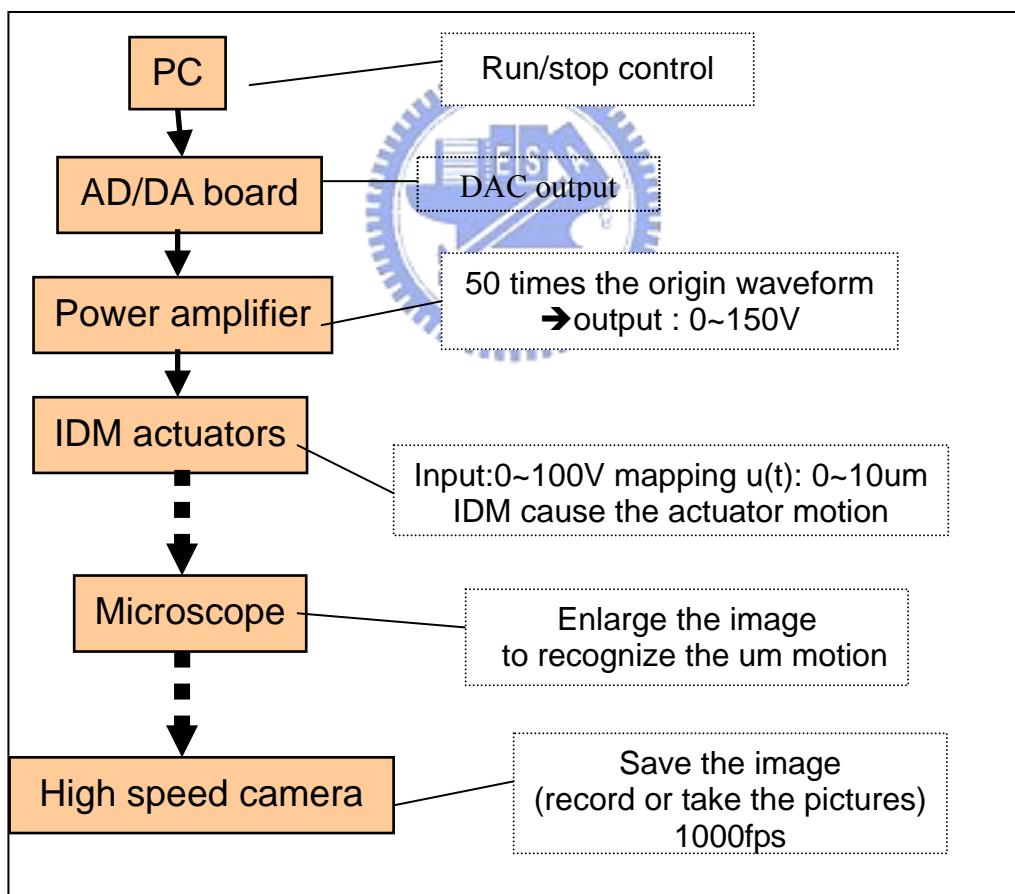


Figure 3.10 The experiment flowchart of 2-D IDM

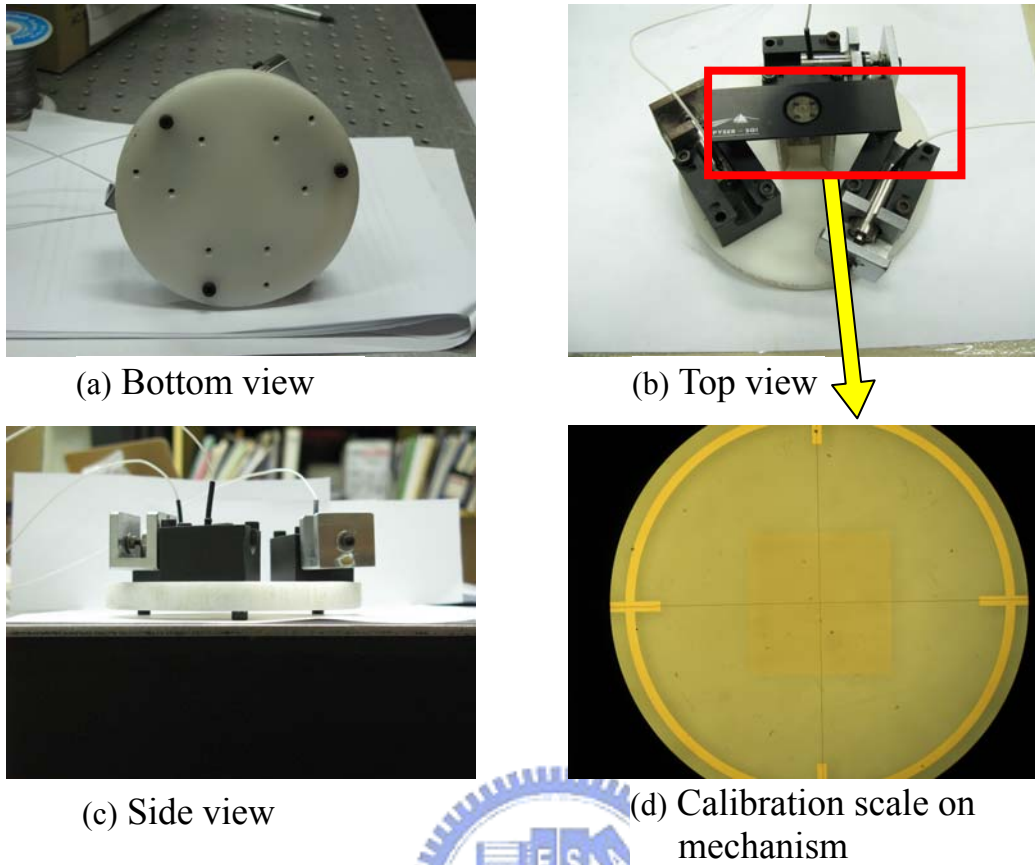


Figure 3.11 The pictures of 2-D IDM

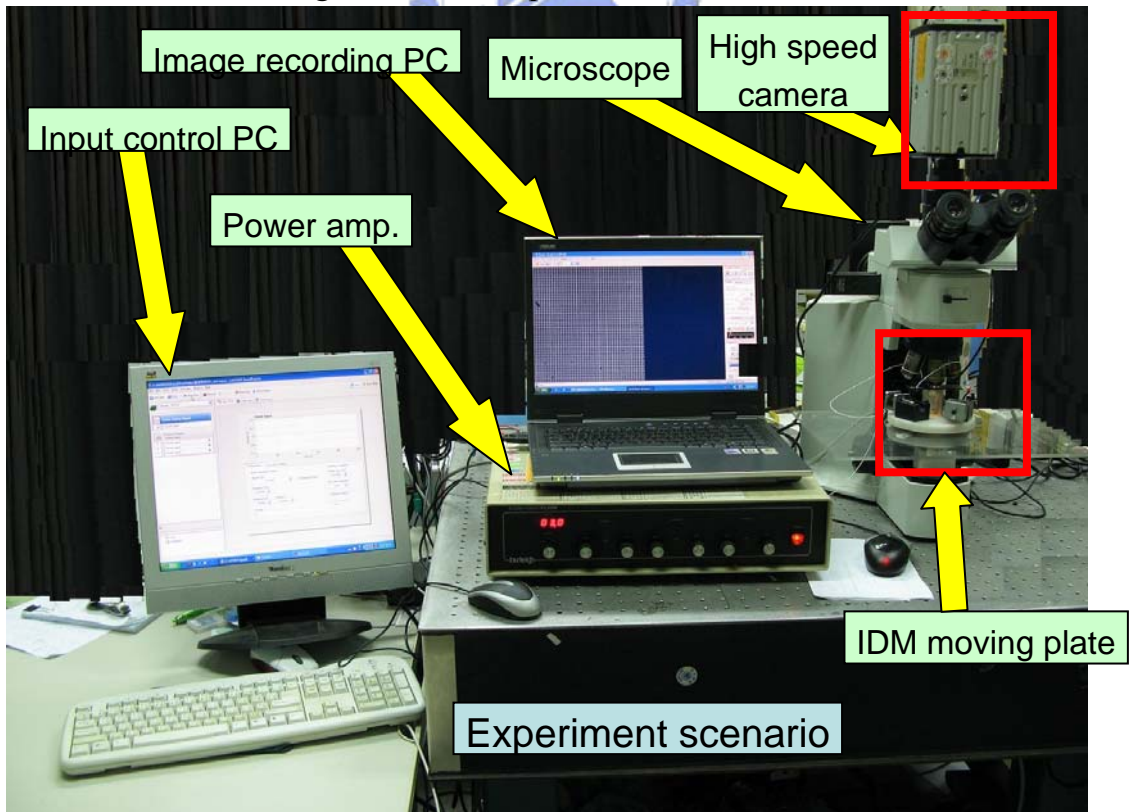


Figure 3.12 2-D IDM experiment scenario

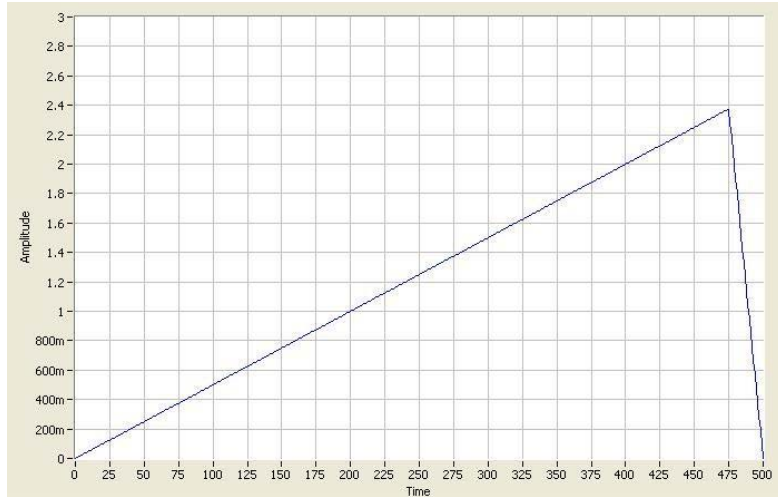


Figure 3.13(a) Forward movement waveform

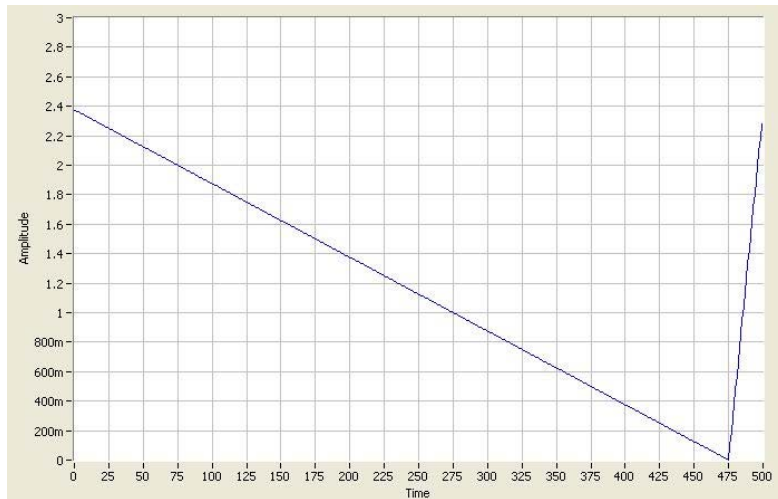


Figure 3.13(b) Backward movement waveform

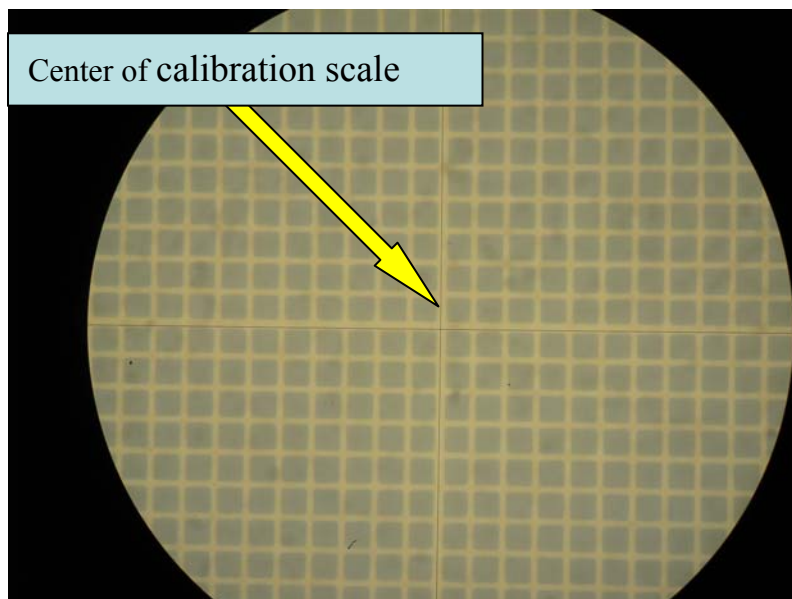


Figure 3.14 View from microscope

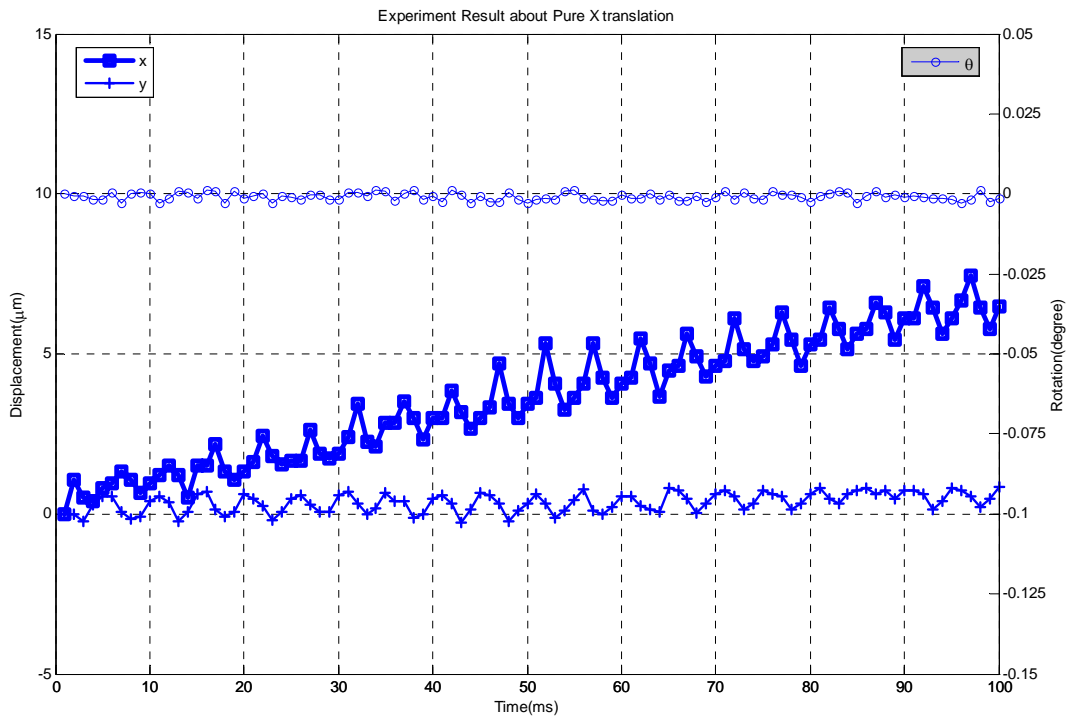


Figure 3.15 Experimental results of pure X translation, 200Hz, 5% duty

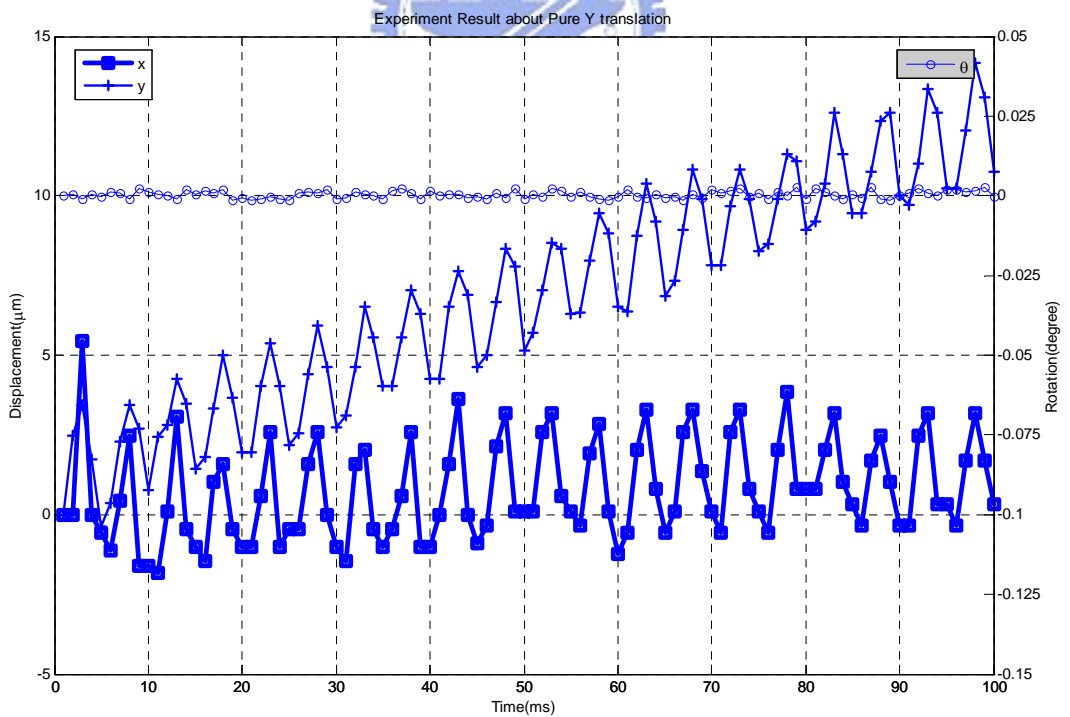


Figure 3.16 Experimental results of pure Y translation, 200Hz, 5% duty

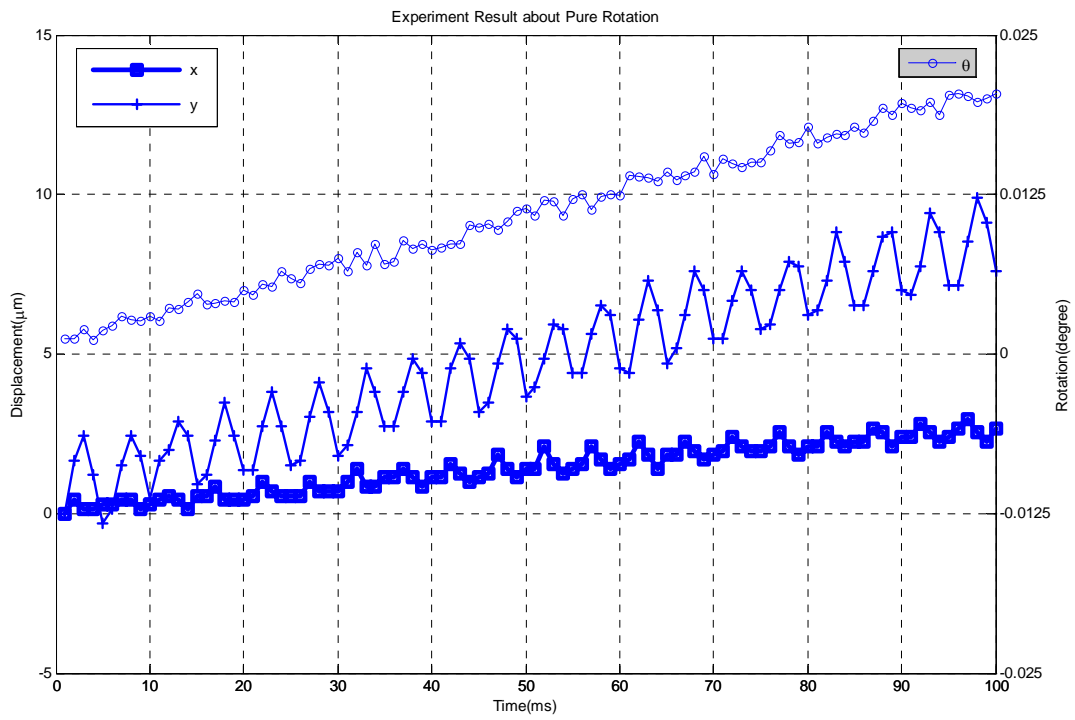


Figure 3.17 Experimental results of pure rotation, 200Hz, 5% duty



M (Kg)	0.25(1-D mechanism) 0.5(2-D mechanism)
R (m)	0.062
m_1, m_2, m_3 (kg)	0.05
c_1, c_2, c_3 (N · t/m)	200
k_1, k_2, k_3 (N/m)	10^7
R_1, R_2, R_3 (m)	0.05
ψ_1 (degree)	90
ψ_2 (degree)	210
ψ_3 (degree)	330
μ	0.3
I (kg · m ²)	0.0008

Table 2.1 The parameters of simulation

Model Number	PA-16/12
Material	Lead zirconate titanate(PZT)
Type	Preloaded stack actuator with housing
Dimension	Piezo stack: rectangular disk 4mm×5mm 0.25mm thickness PZT plate Total stack length: 20mm Housing: φ 12.7mm, length 33.8
Operating Voltage	-20~150V
Motion for 0~100V	-5~23 μ m
Frequency Response	3.5KHz
Nonlinearity	4%
Hysteresis	15%
Creep	Increasing voltage: 1~2% in 20~30sec Decreasing voltage: 7~8% in 60~80 sec

Table 3.1 The specifications of Burleigh's piezoelectric actuator

A/D D/A Board	National instruments PCI-6711: 4 channels output 1 MS/s maximum update rate 24-bit resolution
Power amplifier	Burleigh amplifier PZ-350M 3 channels output Amplification is adjustable Maximum amplification : 50X
Piezo actuators	See Table 3.1
Microscope	Olympus BX51M Eyeglass:10X Objective:5X ,10X ,20X ,100X
High speed camera	X-Stream XS-4 Sensor type: CMOS Maximum resolution: 512*512pixels Memory: 4GB Minimum exposure: 100 ns Frame rate: 5140fps (Max. resolution)

Table 3.2 Detail attribute of experimental apparatus

Step size	Simulation	Experiment	Error
Pure X	0.3631 μ m	0.3243 μ m	10.68%
Pure Y	0.4810 μ m	0.5379 μ m	11.83%
Pure Rotation	0.00091746°	0.00099125°	8.04%

Table 3.3 Comparison between Experiment and simulation